The Histone H3-H4 Tetramer is a Copper Reductase Enzyme

Narsis Attar[1,2,6], Oscar A. Campos[1,2,6], Maria Vogelauer[1,6], Chen Cheng[1], Yong Xue[1], Stefan Schmollinger[3], Nathan V. Mallipeddi[1], Brandon A. Boone[1], Linda Yen[4], Sichen Yang[1], Shannon Zikovich[1], Jade Dardine[1], Michael F. Carey[1,2], Sabeeha S. Merchant[2,3], and Siavash K. Kurdistani[1,2,5,*]

[1]Department of Biological Chemistry, David Geffen School of Medicine, University of California Los Angeles, Los Angeles, CA 90095, USA

[2]Molecular Biology Institute, University of California Los Angeles, Los Angeles, CA 90095, USA

[3]Institute for Genomics and Proteomics, Department of Chemistry and Biochemistry, University of California Los Angeles, Los Angeles, CA 90095, USA

[4]Department of Molecular, Cell, and Developmental Biology, University of California Los Angeles, Los Angeles, CA 90095, USA

[5]Eli and Edythe Broad Center of Regenerative Medicine and Stem Cell Research, David Geffen School of Medicine, University of California Los Angeles, Los Angeles, CA 90095, USA

[6]These authors contributed equally, and are listed alphabetically

*e-mail: skurdistani@mednet.ucla.edu

Abstract

Ancestral histones were present in organisms with small genomes, no nucleus, and little evidence for epigenetic regulation, suggesting histones may have additional older functions. We report that the histone H3-H4 tetramer is an enzyme that catalyzes the reduction of Cu^{2+} to Cu^{1+} when assembled *in vitro* from recombinant histones. Mutations of residues in the putative active site at the interface of the apposing H3 proteins alter the enzymatic activity and cellular processes such as Sod1 function or mitochondrial respiration that depend on availability of reduced copper. These effects are not due to altered gene expression or copper abundance but are consistent with decreased levels of cuprous ions. We propose that the H3-H4 tetramer is an oxidoreductase that provides biousable copper for cellular and mitochondrial chemistry. As the emergence of eukaryotes coincided with the Great Oxidation Event and decreased biousability of metals, the histone enzymatic function may have facilitated eukaryogenesis.

Introduction

Eukaryotes owe their nucleosomal chromatin structure to an ancestral histone-containing archaeon that merged with the protomitochondria, forming the first eukaryotic common ancestor. Archaeal histone tetramers wrap ~60 bp of DNA (Pereira et al., 1997), and have similar geometry and protein-DNA interactions (Mattiroli et al., 2017) as the eukaryotic H3-H4 tetramer. Unlike eukaryotic histones, archaeal histones typically lack extended N-terminal tails, are devoid of post-translational modifications, and occur in organisms with no known protein machinery for epigenetic regulation. Archaea also have significantly smaller genomes than eukaryotes, and do not contain nuclei. With no apparent capability for epigenetic regulation or little need for genome compaction in a confined nuclear space, the possibility arises that the conserved histone H3-H4 tetramer complex may have an additional older function in archaea, and therefore in the eukaryotes that emerged from them.

An overlooked feature of the nucleosome and the geochemical events surrounding eukaryogenesis hinted at what such a function might be. The region of the nucleosome where the two histone H3 proteins form a dimerization interface contains amino acid residues, including cysteine 110 (H3C110) and histidine 113 (H3H113), that are common in transition metal binding sites, particularly those that coordinate copper ions (Katz et al., 2003). These residues display some ability to coordinate transition metal ions *in vitro*, but it is unclear whether such interactions are functionally significant (Adamczyk et al., 2007; Bal et al., 1995; Saavedra, 1986). The evolutionary conservation of residues in this region is greater than expected given their contributions to the thermodynamic stability of the nucleosome (Ramachandran et al., 2011), leading to the suggestion that “a novel function” provided by the H3-H3’ interface is driving the unexpected conservation (Ramachandran et al., 2011). Whether the putative metal-binding

capability of histone H3 is biologically relevant in eukaryotes is not known, but a clue comes from the geochemical history of Earth. The emergence of eukaryotes approximately coincided with the initial accumulation of molecular oxygen (Anbar, 2008). Its increasing abundance substantially altered the biousability of transition metals such as iron and copper in the oceans. These essential metals were also becoming more toxic in the presence of oxygen (Saito et al., 2003), presenting a formidable challenge for their usage. The hypothesis that early eukaryotes may have relied partly on histones for proper metal homeostasis has not been considered.

Copper is an essential element in eukaryotes that serves as a redox co-factor for numerous critical enzymes such as cytochrome *c* oxidase in the mitochondrial electron transport chain (ETC), and Cu, Zn-superoxide dismutases (e.g., Sod1) (Nevitt et al., 2012). Copper also functions as a signaling element to regulate specific biochemical pathways (Krishnamoorthy et al., 2016). In the active sites of redox enzymes, copper cycles between the cupric (Cu^{2+}) and cuprous (Cu^{1+}) forms, including partial oxidation states in between. However, it is the fully reduced cuprous form that is trafficked intracellularly, suggesting a need to maintain cellular cuprous ion pools for proper distribution and utilization of copper (Pufahl et al., 1997). How cells maintain a pool of cuprous ions is not fully understood. Here, we present biochemical, molecular, and genetic data that eukaryotic histone H3-H4 tetramers catalyze reduction of cupric to cuprous ions with the catalytic site likely forming at the H3-H3' interface. Our data indicate that histones provide cuprous ions for utilization by various cellular and mitochondrial proteins. This function may have contributed to the emergence of eukaryotes, making the presence of histones in the ancestral archaeon not incidental (Sandman and Reeve, 1998), but rather essential for eukaryogenesis.

87 **Results**

88 **Recombinant histone H3-H4 tetramer interacts with cupric ions**

89 We first sought to determine whether copper ions interact with the residues at the putative
90 metal-binding site of the H3-H3' interface (Saavedra, 1986) (Figure 1A). We assembled and
91 purified *Xenopus laevis* recombinant histone H3-H4 tetramers (Dyer et al., 2004), which are
92 identical to human H3.2 and H4 histone proteins, respectively (Figure 1 – figure supplement 1A-
93 C). We performed tetramer assembly and subsequent assays in solutions and glassware thoroughly
94 depleted of contaminating metal ions, a critical precaution for *in vitro* studies (see Methods).

95 We focused first on the role of the pair of cysteine residues at position 110 (H3C110), one
96 from each apposing H3 protein (Adamczyk et al., 2007; Saavedra, 1986), in copper ion binding.
97 H3C110 is present in the canonical histone H3 of 146 out of 166 eukaryotes that span the major
98 kingdoms (Macadangdang et al., 2014), including *X. laevis*, and *H. sapiens.* It is the sole cysteine
99 residue present in most H3s or in H4 and is absent only in a few fungi of the genus Saccharomyces,
100 including *S. cerevisiae* H3 (Figure 1B). Cysteine-copper ion interactions generally result in
101 characteristic absorption spectra in the UV-visible range that are dependent on the coordination
102 environment (Solomon et al., 1993). Incubation of the *X. laevis* wildtype (Xl WT) tetramer with
103 increasing molar equivalents of Cu^{2+} resulted in an increasing UV absorbance band with a peak at
104 245 nm that plateaued at a tetramer to cupric ion ratio of 1 (Figure 1C, left panel). Critically,
105 mutation of C110 to alanine (*H3C110A*), which did not affect tetramer assembly (Figure 1 – figure
106 supplement 1B and C), abolished this copper-dependent absorbance change (Figure 1C, right
107 panel), consistent with a direct interaction between C110 and a copper ion. Furthermore, when
108 assayed by Immobilized Metal Affinity Chromatography (IMAC) using a Cu^{2+}-loaded resin, the

109 Xl WT tetramer exhibited substantially more retention than the H3^{C110A} tetramer, corroborating the
110 role of H3C110 in tetramer-copper ion interaction (Figure 1D).
111
112 **The histone H3-H4 tetramer is a cupric ion reductase**
113 We next hypothesized that the H3-H4 tetramer may not only bind copper but function as
114 an oxidoreductase, catalyzing the reduction of Cu^{2+} to Cu^{1+} in the presence of a source of electrons.
115 We developed a colorimetric assay to measure the production of Cu^{1+} by utilizing copper chelators
116 neocuproine (NC) or bicinchoninic acid (BCA) to detect Cu^{1+} quantitatively (Figure 2A, Figure 2
117 – figure supplement 1, and Figure 2 – figure supplement 2A and B). Formation of the NC_2-Cu^{1+}
118 or the BCA_2-Cu^{1+} complex result in a change in absorbance at 448 nm or 562 nm, respectively.
119 The assay also contained reduced forms of tris(2-carboxyethyl)phosphine (TCEP), nicotinamide
120 adenine dinucleotide (NADH), or its phosphate form (NADPH) as electron donors. Reactions were
121 initiated by addition of Cu^{2+} substrate in the form of a $CuCl_2$-Tricine, $CuCl_2$-N-(2-
122 Acetamido)iminodiacetic acid (ADA), or $CuCl_2$-Nitrilotriacetic acid (NTA) solution, upon which
123 spontaneous Cu^{1+} production occurred at a slow rate in control buffers (Figure 2B). In contrast,
124 the rate of Cu^{1+} production was substantially increased when reactions were performed in the
125 presence of the Xl WT tetramer (Figure 2B). Production of Cu^{1+} plateaued at later time points due
126 to near full consumption of the electron donor with ~75% of total Cu^{1+} produced in the first 30
127 seconds (Figure 2B). Importantly, the rate of Cu^{1+} production was decreased to near-background
128 levels upon heat-inactivation of the Xl WT tetramer (Figure 2B). The unassembled *X. laevis*
129 histone H3 on its own or another histone, the yeast H2A, did not enhance cupric ion reduction
130 (Figure 2 – figure supplement 2C). Digestion of the H3-H4 tetramer with Proteinase K prior to the
131 assay abolished cupric reductase activity (Figure 2C), confirming the importance of the structural

132 conformation of the tetramer for copper reduction. No significant production of Cu^{1+} occurred in
133 the absence of TCEP and increasing rates of production occurred with increasing amounts of either
134 TCEP (Figure 2D) or Cu^{2+} (Figure 2E), eventually approaching a maximum rate of reduction
135 which is consistent with protein-based catalysis (Figure 2 – figure supplement 2D and E). The
136 tetramer also enhanced the rate of cupric ion reduction with NADPH, albeit in a different reaction
137 condition that was necessary to decrease un-catalyzed copper reduction by NADPH (Figure 2F).

138 The *C110A* mutation in Xl H3 substantially reduced the rate of cupric ion reduction (Figure
139 2G). Treatment of the Xl WT tetramer with *N*-ethylmaleimide (NEM) to irreversibly inhibit
140 H3C110 reactivity abolished Cu^{1+} production (Figure 2H), corroborating the importance of
141 H3C110 in cupric ion reduction. Given the general ability of thiols to reduce cupric ions *in vitro*
142 (Pecci et al., 1997), we considered whether any set of protein or small molecule thiol groups may
143 enhance the rate of cupric ion reduction by TCEP, as opposed to merely donating electrons directly
144 to Cu^{2+}. Reactions carried out in the presence of RNase A, which contains eight redox reactive
145 cysteines capable of forming four disulfide bonds (Klink et al., 2000), at the same concentration
146 as the tetramer did not enhance the rate of copper reduction (Figure 2 – figure supplement 2F).
147 Similarly, 1 μM of DTT directly reduced an equimolar 2 μM of Cu^{2+} but did not substantially
148 enhance the rate of cupric ion reduction by TCEP (Figure 2 – figure supplement 2F), emphasizing
149 the unique role of H3C110 in the structural context of the H3-H4 tetramer for enzymatic activity.

150 The pair of histidine residues at position 113 (H3H113) at the H3-H3' interface have also
151 been proposed to participate in metal coordination (Adamczyk et al., 2007; Saavedra, 1986). This
152 highly conserved residue is present in the canonical histone H3 of all 166 eukaryotes that span the
153 major kingdoms (Macadangdang et al., 2014), as well as in the structurally-equivalent position of
154 most (29 out of 33) archaeal histones spanning the major phyla (Henneman et al., 2018) (Figure

155 1A and B). Thus, we asked whether the H3H113 residue also enables the H3-H4 tetramer to
156 enhance the rate of cupric ion reduction. Mutation of H3H113 to alanine (*H3H113A*) or to
157 asparagine or tyrosine (*H3H113N* or *H3H113Y*), which have been found in certain cancers (Forbes
158 et al., 2015), had little effect on the rate of reduction with Cu^{2+}-Tricine as the substrate (data not
159 shown) but diminished cupric ion reduction in reactions with Cu^{2+}-ADA (Figure 2I and Figure 2
160 – figure supplement 2G) or Cu^{2+}-NTA as Cu^{2+} substrates (Figure 2 – figure supplement 2H and I).
161 The differing effects of ADA, NTA, and Tricine on copper reduction rates are likely due in part to
162 their differing Cu^{2+} coordination ability and/or geometry. Altogether, our data reveal that the H3-
163 H4 tetramer uses electron donors as cofactors to catalyze Cu^{2+} reduction and is thus an
164 oxidoreductase enzyme.

165 The histone H3 of *S. cerevisiae* naturally lacks the C110 residue found in most other
166 eukaryotic H3s, and instead contains an alanine at this position (Figure 1B). It does, however,
167 contain the H3H113 residue at the H3-H3' interface. As expected, recombinant yeast H3-H4
168 tetramer did not absorb UV energy in the 245 nm range when incubated with Cu^{2+} (see below), as
169 this was associated with the H3C110-copper ion interaction (Figure 1C). However, a broad peak
170 centered at 680 nm was observed with increasing molar equivalents of Cu^{2+}, which required high
171 concentrations of yeast tetramer, consistent with weakly-absorbing d-d transitions that are typical
172 of coordinated Cu^{2+} ions (Mesu et al., 2006) (Figure 3A, left panel). Notably, this absorbance band
173 only occurred when the yeast tetramer was assembled and incubated with Cu^{2+} ions in the presence
174 of 2 M NaCl, but not at lower ionic strengths (data not shown), which may interfere with the
175 structural conformation of the yeast tetramer (Lee et al., 1982). The *H113A* mutation in the yeast
176 H3, which did not affect tetramer assembly (Figure 3 – figure supplement 1A and B), strongly
177 reduced copper-dependent absorbance change at 680 nm (Figure 3A, right panel), consistent with

178 the role of the histidine in copper ion interaction independently of the H3C110 residue. The yeast
179 H3-H4 tetramer also exhibited substantial retention on the Cu^{2+} IMAC column, which was reduced
180 in tetramers harboring the *H3H113A, N,* or *Y* mutations (Figure 3B and Figure 3 – figure
181 supplement 1A-D).

182 Mutation of yeast H3A110 to cysteine (yH3^{A110C} tetramer) (Figure 3 – figure supplement
183 1E and F) elicited a copper-dependent absorbance band centered at 245 nm, nearly identical to that
184 observed with the *X. laevis* tetramer (Figure 3C), corroborating the ability of the yeast tetramer to
185 interact with copper ions at the H3-H3' interface. Furthermore, the *H3H113A* mutation in the
186 context of the yeast H3^{A110C} tetramer (yH3^{A110CH113A} tetramer) (Figure 3 – figure supplement 1E
187 and G) resulted in diminished copper-dependent absorbance at 245 nm (Figure 3C), indicating that
188 H3H113 affects the nature of the cysteine-copper ion interaction. Like the *X. laevis* tetramer, the
189 yeast H3^{A110C}-H4 tetramer displayed cupric reductase activity, which was diminished by the
190 *H3H113A* mutation (Figure 3D). In the absence of the H3C110 residue, the yeast tetramer did not
191 display robust cupric reductase activity in standard salinity (~100-150 mM NaCl) likely due to
192 deficient Cu^{2+} binding, unsatisfactory yeast tetramer conformation and/or inadequate
193 reconstitution of the cellular environment in our assay conditions. We also could not perform
194 copper reduction assays in high (2 M) NaCl concentrations, at which the yeast tetramer interacts
195 with Cu^{2+} (Figure 3A), due to salt interference with other assay components. Nonetheless, our
196 findings suggest that the yeast H3-H4 tetramer can display cupric reductase activity, and that the
197 H3H113 residue participates in this function.

198 *(Note to reviewers: We have attempted to perform the curpric reductase assay with*
199 *nucleosomes. However, the combination of Cu^{2+}, the copper chelator, and DNA form an insoluble*

200 *complex, precluding us from performing enzyme assays. We are working on this problem but may*
201 *or may not make a breakthrough in a reasonable timeframe.)*
202
203 **Mutation of histone H3 histidine 113 results in loss of function in yeast**
204 We next investigated whether mutation of the H3H113 residue *in vivo* would produce
205 cellular effects consistent with the ability of histone H3 to produce Cu^{1+} ions. Mutation of H3H113
206 to alanine was lethal in *S. cerevisiae* (Huang et al., 2009) (Figure 4A). However, introduction of
207 either *H3H113N* or *H3H113Y* mutations in the two chromosomal copies of the histone H3 gene
208 generated viable yeast strains $H3^{H113N}$ and $H3^{H113Y}$, albeit with slower growth rates compared to
209 WT (Figure 4B). Although replacement of H3H113 with any of three residues resulted in loss of
210 copper binding by the H3-H4 tetramers *in vitro*, we sought to rule out the possibility that the slow
211 growth phenotypes were due to gain of a toxic function *in vivo*. Yeast strains in which the
212 *H3H113N* and *H3H113Y* mutant histones were expressed from only one locus, with the other locus
213 deleted, were severely sick compared to strains expressing both histone copies (Figure 4C),
214 confirming that substitution of H3H113 with specific amino acids generates loss-of-function
215 alleles.
216
217 **H3H113 mutations lead to de-repression of Mac1 target genes**
218 We next examined whether the *H3H113N* or *H3H113Y* mutations result in decreased
219 cuprous ion availability. We first investigated the activity of the transcription factor Mac1 because
220 it is directly inhibited by cuprous ions in the nucleus (Graden and Winge, 1997). Global gene
221 expression analysis by mRNA-seq revealed largely similar profiles in WT and $H3^{H113N}$ strains in
222 rich fermentative medium (YPD and SC) (Figure 5 – figure supplement 1). However, Mac1 target

223 genes displayed increased expression in *H3*^{H113N} compared to WT (Figure 5A), which was
224 corroborated in the *H3*^{H113Y} strain via gene-specific RT-qPCR analysis (Figure 5B). Deletion of
225 *CTR1*, the main copper importer in yeast (Dancis et al., 1994), expectedly resulted in upregulation
226 of Mac1 target genes (Figure 5A). However, Mac1 target genes showed greater upregulation as
227 well as incomplete repression in response to exogenous copper in *H3*^{H113N}*ctr1*Δ compared to *ctr1*Δ
228 (Figure 5C). Importantly, although *ctr1*Δ substantially reduced total intracellular levels of copper,
229 they were unchanged in strains with the *H3H113N* mutation compared to strains with WT H3
230 (Figure 5D). This finding suggests that the effect of H3H113 mutations on Mac1 activity is not
231 due to altering copper abundance but is consistent with decreased availability of cuprous ions in
232 the nucleus.
233

234 **The H3H113 residue is required for efficient use of copper for mitochondrial respiration**

235 We next tested whether mutation of H3H113 impacts mitochondrial respiration, which
236 depends on copper ions for cytochrome *c* oxidase function. Although *H3*^{H113N} did not display a
237 defect in mitochondrial respiration, the more defective *H3*^{H113Y} strain displayed a significant loss
238 of cellular O_2 consumption in respiratory media where glucose was replaced with the non-
239 fermentable ethanol and glycerol (YPEG) (Figure 6A), consistent with its greater defect in Mac1
240 repression (Figure 5B). This defect was exacerbated in copper depleted medium, which was
241 achieved by addition of the copper chelator bathocuproinedisulfonic acid (BCS), and was
242 recovered by excess exogenous copper (Figure 6B), suggesting that copper utilization is perturbed
243 when H3H113 is mutated.

244 To relate defects in mitochondrial respiration to disruption of copper utilization, we
245 assessed the ability of cells to increase respiratory function as they were shifted from a copper

246 depleted state to a copper replete state. As expected, copper depletion via *CTR1* deletion resulted
247 in a low rate of O_2 consumption which was gradually increased by addition of copper exogenously
248 (Figure 6C). However, substantially more exogenous copper was required to rescue *ctr1*Δ in the
249 context of the *H3H113N* mutant histone (Figure 6C). The O_2 consumption measured in our assays
250 was almost entirely abolished by treatment with antimycin A (Figure 6 – figure supplement 1A),
251 an inhibitor of cytochrome *c* reductase, reaffirming the specific impact of the *H3H113N* mutation
252 on mitochondrial respiration. $H3^{H113N}$*ctr1*Δ also displayed reduced recovery of copper-dependent
253 cytochrome *c* oxidase activity compared to *ctr1*Δ (Figure 6D). The deficiencies in the context of
254 *H3H113N* were apparent at early times after inoculation in liquid medium before any measurable
255 growth had occurred, suggesting that they were not merely consequences of diminished growth
256 rate. *CTR1* deletion abolished respiratory growth on YPEG, which was partially rescued by
257 exogenous copper. Substantially more exogenous copper was required to rescue growth of *ctr1*Δ
258 in the context of the *H3H113N* or *H3H113Y* mutant histones (Figure 6E and Figure 6 – figure
259 supplement 1B). Combination of *H3H113N* with deletion of *MAC1*, which is required for *CTR1*
260 expression (Graden and Winge, 1997), also increased the amount of exogenous copper required
261 for growth on YPEG compared to *mac1*Δ alone (Figure 6 – figure supplement 1C). Addition of
262 iron, zinc, or manganese did not rescue the growth defects of *ctr1*Δ strains, confirming that the
263 respiratory deficiencies were specifically due to insufficient copper utilization (Figure 6 – figure
264 supplement 1D).

265 Consistent with the hypomorphic nature of the *H3H113N* mutation, a strain with one WT
266 histone H3 and one containing the *H113N* mutation revealed a partial loss of function in copper
267 utilization that was intermediate to that of strains containing two *H3H113N* or two WT H3 genes
268 (Figure 6F). Furthermore, we tested whether a lower dosage of nucleosomes would also disrupt

269 copper utilization by deleting one of the two copies of the histone H3 and H4 genes (*hht1-hhf1*Δ)
270 in an otherwise WT cell. Accordingly, *hht1-hhf1*Δ displayed decreased cellular H3 and H4 protein
271 content and increased chromatin accessibility by Micrococcal nuclease (MNase) (Figure 6 – figure
272 supplement 2) but did not affect growth in YPD (Figure 6G). Importantly, *hht1-hhf1*Δ increased
273 the requirement of copper in *ctr1*Δ for growth in YPEG medium (Figure 6H).
274

275 **Disruptions in copper utilization by H3H113 mutations are not accounted for by changes in**
276 **chromatin function, cellular copper levels, extracellular metal reduction, or glutathione**
277 **levels**

278 Our findings are consistent with H3H113 mutants impacting cuprous ion availability, but
279 we considered whether potential disruptions in chromatin structure or gene regulation account for
280 the copper utilization defects as opposed to direct interactions of the histones with copper ions.
281 Deletion of Asf1, a histone chaperone that facilitates nucleosome assembly in part through
282 interaction with H3H113 (Adkins et al., 2004; Agez et al., 2007), or the *H3H113N* mutation
283 resulted in minimal disruption of chromatin accessbility compared to WT as assessed by MNase
284 digestion (Figure 6 – figure supplement 3A). Importantly, any potential disruption of chromatin
285 structure did not account for the increased requirement for copper, as *asf1*Δ did not phenocopy the
286 H3H113 mutants in respiratory media (Figure 6 – figure supplement 3B). Global gene expression
287 patterns were similar between WT and $H3^{H113N}$ strains in respiratory media (Figure 6 – figure
288 supplement 3C), with comparable upregulation of genes involved in the electron transport chain,
289 tricarboxylic acid cycle, and copper and iron regulation (Figure 6 – figure supplement 3D and E).

290 We also considered whether changes in the total availability of copper ions could account
291 for the defect in *H3H113N* as opposed to impacts on just the cuprous species. As was the case in

292 fermentative YPD medium (Figure 5C), total intracellular levels of copper were not lower in
293 *H3*^{H113N} compared to WT in respiratory YPEG medium, although a slight decrease in iron in YPEG
294 was observed (Figure 6 – figure supplement 4A). Addition of excess copper in YPEG, which
295 rescued mitochondrial respiration in *ctr1*Δ but not in *H3*^{H113N}*ctr1*Δ (Figure 6 – figure supplement
296 1B), increased intracellular levels of copper similarly in both strains (Figure 6 – figure supplement
297 4A). These findings indicate that the defect in copper utilization in *H3*^{H113N}*ctr1*Δ was not due to
298 deficient copper uptake through the remaining minor copper importers, such as Fet4 (Hassett et
299 al., 2000). Lastly, inefficient recovery of *ctr1*Δ in the context of *H3H113N* was not due to increased
300 sequestration of copper ions by the metallothionein Cup1 since loss of Cup1 (*cup1*^{F8stop}) had no
301 effect on the requirement for copper in *H3*^{H113N}*ctr1*Δ (Figure 6 – figure supplement 4B).
302 We next asked whether the known extracellular metalloreductases *FRE1* and *FRE2*
303 (Hassett and Kosman, 1995) might increase the copper requirement similar to the H3H113
304 mutations. Deletion of both FRE genes did not phenocopy the H3H113 mutations, however,
305 (Figure 6 – figure supplement 5A), indicating that an inability to maintain intracellular rather than
306 extracellular cuprous ions results in copper-dependent respiratory deficiency. Furthermore, we
307 examined how the H3H113 mutations would compare to the effect of decreasing cellular levels of
308 glutathione (GSH), which participates in cellular copper metabolism (Freedman et al., 1989).
309 Decreasing GSH abundance, by deleting the gamma glutamylcysteine synthetase gene (*GSH1*),
310 increased the amount of copper required to rescue *ctr1*Δ in the context of *gsh1*Δ but to a lesser
311 extent than the *H3H113N* mutation (Figure 6 – figure supplement 5B). Combining *H3H113N* with
312 *gsh1*Δ caused an even greater defect in copper utilization (Figure 6 – figure supplement 5B),
313 suggesting that the histones impact cuprous ion utilization in a different manner than GSH.
314

315 **Histone H3 is required for efficient utilization of copper for Sod1 function.**

316 We next considered whether the impact of histone H3 on cuprous ion availability and
317 copper-dependent function extends to the yeast Sod1. An in-gel superoxide dismutase assay
318 (Leitch et al., 2009) demonstrated that total Sod1 activity was ~40% less in $H3^{H113Y}$ compared to
319 WT when grown in rich medium, which was recovered by addition of 50 μM copper (Figure 7A
320 and Figure 7 – figure supplement 1A). *H3H113N* also decreased Sod1 activity by ~20% compared
321 to WT (Figure 7B). Deletion of *CTR1* reduced Sod1 activity and formation of its internal disulfide
322 bond, which are both dependent on the presence of cuprous ions and on the copper chaperone for
323 Sod1, Ccs1 (Furukawa et al., 2004). Combining *ctr1*Δ with *H3H113N* further decreased the
324 internal disulfide bond and substantially lowered Sod1 activity to ~10% of WT. Both Sod1 activity
325 and its disulfide bond were restored to wildtype levels by addition of excess exogenous copper
326 (Figure 7B).

327 Loss of function of *SOD1* or *CCS1* causes lysine auxotrophy in yeast when grown in the
328 presence of oxygen (Lin and Culotta, 1996). Consistent with this, $H3^{H113N}$*ctr1*Δ exhibited a growth
329 defect in lysine deficient conditions (Figure 7C). Further limiting copper abundance by addition
330 of the copper chelator BCS rendered $H3^{H113N}$*ctr1*Δ, but not *ctr1*Δ, auxotrophic for lysine even in
331 the presence of wildtype *CCS1* and *SOD1* genes (Figure 7C). Together, these data are consistent
332 with a deficiency in copper utilization for Sod1 function when H3H113 is mutated.

333 We also assessed the ability of cells to restore copper-dependent Sod1 function starting
334 from a state of low activity due to low delivery of copper ions. Copper delivery to Sod1 was first
335 diminished by deleting *CCS1*, which significantly decreased Sod1 activity (Figure 7D). Sod1
336 activity in the absence of Ccs1 was increasingly restored by addition of excess copper in rich
337 medium (Figure 7D). Importantly, the *H3H113N* mutation increased the amount of copper required

338 to restore Sod1 activity in *ccs1*Δ (Figure 7D). Correspondingly, the lysine auxotrophy of *ccs1*Δ
339 was rescued by addition of excess exogenous copper (Figure 7E). However, substantially more
340 copper was required to rescue *ccs1*Δ in the context of the *H3H113N* mutation (Figure 7E).
341 Interestingly, unlike the effect of *H3H113N*, deletion of *CTR1* did not further increase the
342 requirement of *ccs1*Δ for exogenous copper (Figure 7 – figure supplement 1B), suggesting that
343 histone H3 contributes to copper utilization in a qualitatively different manner than Ctr1. Excess
344 copper did not rescue the lysine auxotrophy of *sod1*Δ strains, confirming that Sod1 is required for
345 copper-dependent lysine prototrophy (Figure 7 – figure supplement 1C). Hypoxia rescued the
346 lysine auxotrophy of *ccs1*Δ and *sod1*Δ in both WT and $H3^{H113N}$ (Figure 7 – figure supplement 1D),
347 indicating that the copper utilization defect for lysine prototrophy in *H3H113N* strains only
348 manifests when Sod1 function is required.

349 The *H3H113N* mutation specifically disrupts copper utilization as addition of manganese,
350 zinc, or iron did not rescue *ccs1*Δ lysine auxotrophy (Figure 7 – supplement 1E). The increased
351 copper requirement of $H3^{H113N}ccs1$Δ was not due to differences in Cup1-dependent copper
352 sequestration (Figure 7 – figure supplement 2A) or intracellular copper and iron levels (Figure 7 –
353 figure supplement 2B and C). As with respiratory growth, deletion of *ASF1* had no effect on the
354 copper-dependent rescue of *ccs1*Δ (Figure 7F). Global gene expression also did not account for
355 the defective copper utilization as *ccs1*Δ and $H3^{H113N}ccs1$Δ displayed similar patterns (Figure 7 –
356 figure supplement 2D), including genes involved in lysine biosynthesis, copper homeostasis, and
357 antioxidant defense (Figure 7 – figure supplement 2E and F). Altogether, our findings reveal that
358 the H3H113 residue is also important for copper utilization by Sod1. The significant impacts of
359 H3H113 mutations in at least two separate copper-dependent processes support the model that the

360 interaction of copper ions and the putative cupric reductase function of the yeast histone H3 impact
361 cuprous ion availability in the cell.
362
363 **The *H3A110C* mutation enhances copper utilization for respiratory growth.**
364 The ability of H3C110 to enhance copper reductase activity of the yeast tetramer *in vitro*
365 suggested that the *H3A110C* mutation should enhance cuprous ion availability and copper
366 utilization *in vivo*. We generated the yeast $H3^{A110C}$ strain, with the *H3A110C* mutation in both
367 *HHT1* and *HHT2* genes in their chromosomal loci. This strain grew similarly to WT cells in rich
368 respiratory medium (Figure 8A). However, in contrast to the effects of the H3H113 mutations, the
369 *H3A110C* mutation enhanced the ability of exogenous copper to restore the growth of *ctr1*Δ in
370 YPEG, consistent with more efficient copper utilization for mitochondrial respiration (Figure 8B).
371 We reasoned that increased provision of cuprous ions, due to the enhanced cupric ion reduction
372 caused by the *H3A110C* mutation, may mitigate the depletion of cellular GSH. Indeed,
373 $H3^{A110C}$*gsh1*Δ grew better than *gsh1*Δ in copper-depleted respiratory conditions (Figure 8C) with
374 a greater O_2 consumption rate (Figure 8D). Furthermore, $H3^{A110C}$ exhibited a growth advantage
375 upon addition of a toxic but sub-lethal amount of potassium cyanide (KCN), a potent inhibitor of
376 the copper-dependent cytochrome *c* oxidase independently of GSH levels, especially upon
377 addition of exogenous copper (Figure 8E and F). These results highlight the advantage in copper
378 utilization conferred by the *H3A110C* mutation. Moreover, the presence of the *H3A110C* mutation
379 significantly rescued the copper utilization defect of the $H3^{H113N}$*ctr1*Δ strain (Figure 8G). Lastly,
380 the presence of the *H3A110C* mutation rescued the lethality of the *H3H113A* mutation (Figure 8H),
381 corroborating the opposing effects of the H3A110 and H3H113 mutations both *in vivo* and *in vitro*.
382 These findings further support that histone H3 contributes to cellular copper utilization, likely

383 through the maintenance of the cuprous ion pool via catalytic conversion of cupric to cuprous
384 species.
385
386 **Discussion**
387 Since their identification, histones have been considered to serve as packaging and
388 regulatory proteins for the eukaryotic genome. We now reveal the eukaryotic histone H3-H4
389 tetramer as a cupric reductase that provides cuprous ions for cellular and mitochondrial biology.
390 The enzymatic activity of the H3-H4 tetramer suggests the protein complex has novel features,
391 including a catalytic site, that were previously unsuspected. The structural features, unusual
392 evolutionary conservation, and our biochemical data suggest that a likely site for the catalytic
393 pocket is at the interface of the two H3 proteins. Subsequent studies should determine the
394 mechanisms by which the residues in this region, including H113 and C110, contribute to direct
395 cupric ion binding, increasing its reduction potential, and promoting electron transfer (Liu et al.,
396 2014). The H3-H3' interface forms *in vivo* only during nucleosome assembly on DNA and can
397 remain accessible by molecules in the surrounding environment (Feinstein and Moudrianakis,
398 1986). Therefore, the commencement of enzymatic activity would be inextricably coupled to the
399 protection of DNA as it wraps on the outer surface of the nucleosome away from the putative
400 binding site. Such a coupling may be a beneficial adaptation in species that require provision of
401 reduced copper, as it would also decrease the potentially coinciding damage due to copper.
402 How the tetramer extracts electrons from a reducing co-factor(s) is unclear, as is the
403 location at which this occurs. Electrons could transfer directly to the tetramer-bound copper from
404 co-factors or through the protein in a mechanism involving a chain of residues in transient redox
405 states (Lucas et al., 2011; Williams et al., 1997). In this regard, whether the sequence differences

406 between the histone H3 variants or post-translational modifications of the histones influence the
407 kinetic properties or co-factor requirements of the H3-H4 tetramer enzyme activity remain
408 interesting and open questions.

409 Since cellular copper ions are mostly bound by proteins (Rae et al., 1999), copper is likely
410 delivered to and taken away from histones through as-yet-to-be-identified chaperones. Copper is
411 present in the nucleus but the dynamics of its entry and exit or its function(s) are unclear (McRae
412 et al., 2013; Yang et al., 2005). Interestingly, when cellular copper efflux is compromised such as
413 in Wilson disease, copper disproportionately accumulates in the nucleus, reaching millimolar
414 concentrations (Burkhead et al., 2011; Huster et al., 2006), albeit likely bound to chaperones.
415 Considering the importance of copper to processes as diverse as tissue integrity, methylation cycle,
416 iron homeostasis, and melanin and neurotransmitter syntheses in mammals (Finney et al., 2014;
417 Nevitt et al., 2012; Winston and Jaiser, 2008), the enzymatic activity of histones could have wide-
418 ranging effects at molecular, cellular, and tissue levels with consequences for organismal
419 physiology and disease.

420 The oxidoreductase function of the H3-H4 tetramer, the ancient structural form of histones,
421 could provide a reasonable explanation for why the archaeal ancestor of the eukaryotes possessed
422 histone tetramers. This enzymatic activity, together with an associated intracellular Cu^{1+} transit
423 system, could have facilitated the provision of cuprous ions to the nascent mitochondria to
424 maintain a functioning ETC thereby intimately linking histones to the successful emergence of our
425 common eukaryotic ancestor.

426

427 **Materials and Methods**

428 Statistical methods were not used to determine sample size. The investigators were not blinded to
429 the identity of strains and samples in experiments and analysis.

430

431 **Strains and general growth conditions.** *Saccharomyces cerevisiae* strains used in this study are
432 based on the BY4741 (S288C background, MATa) (Brachmann et al., 1998) and RMY102 (MATa)
433 (Mann and Grunstein, 1992) strains and are listed in Table 1. Strains based on BY4741 were
434 maintained on YPD (1% Yeast extract, 2% Peptone, 2% Glucose) plates, and which were
435 supplemented with 20 μM $CuSO_4$ for strains lacking *CTR1*. Furthermore, strains lacking *CTR1*
436 were used for experiments within three passages to avoid emergence of potential mutants with
437 enhanced ability for acquisition of copper through alternative routes. Strains based on RMY102
438 were maintained on SG-trp-ura (Synthetic complete medium, lacking tryptophan and uracil, and
439 with 2% Galactose) plates. All strains were grown at 30°C in all experiments as described below.
440 Bacteria for histone expression were BL21(DE3)pLysS and BL21(DE3) cells (Agilent).
441 Transformed bacteria were grown on 2xTY media (1.6% Bacto Tryptone, 1% Yeast Extract, 0.5%
442 NaCl) supplemented with 100 μg/mL ampicillin.

443

444 **Strain generation for yeast experiments.** *BY4741 background:* The histone H3 *H113N* mutation
445 was generated in both chromosomal loci (*HHT1* and *HHT2*) in a stepwise and marker-less manner.
446 First, using the *delitto perfetto* approach (Storici and Resnick, 2006), the *H113N* mutation was
447 introduced into the *HHT2* locus. Second, the *H113N* mutation was introduced in *HHT1* using the
448 CRISPR-Cas9 system optimized for *S. cerevisiae* (Ryan et al., 2014). The pCAS plasmid,
449 containing both the Cas9 gene from *Streptococcus pyogenes* and a single guide RNA, was a gift

450 from Jamie Cate (Ryan et al., 2014). The histone H3 *H113Y* and *A110C* mutations were introduced
451 in a similar manner as described but CRISPR-Cas9 was used for both HHT1 and HHT2.
452 Subsequent gene deletions and promoter insertions were generated by standard yeast gene
453 replacement and targeted insertion methodology using selectable marker integration (Goldstein
454 and McCusker, 1999; Longtine et al., 1998). Additionally, *CTR1* was deleted in several strains
455 using the CRISPR-Cas9 targeting system. Successful integrations and deletions were confirmed
456 by PCR. The CUP1 gene was disrupted by introduction of a stop codon at Phe8 at all CUP1 copies
457 using the CRISPR-Cas9 system as described above for generating histone mutants.
458 *RMY102 background:* The histone H3 *H113N*, *H113A*, and *A110C* mutations were introduced into
459 the *HHT2* gene of the pRM200 plasmid (CEN4/ARS1/TRP1/HHT2-HHF2) (Mann and Grunstein,
460 1992) by site directed mutagenesis (QuikChange, Agilent). The WT or mutagenized pRM200
461 plasmids were then introduced into the RMY102 strain by standard yeast transformation
462 procedures, and cells were maintained on media lacking both tryptophan and uracil to ensure the
463 presence of both pRM102 (CEN4/ARS1/URA3/p^{GAL1}-HHT2-p^{GAL10}-HHF2) and pRM200
464 plasmids.
465
466 **Plasmids for histone expression.** Plasmids for expression of *Xenopus laevis* histones are from
467 (Luger et al., 1997). All sequence changes to the plasmid were accomplished by site directed
468 mutagenesis (QuikChange, Agilent). The histone H3 plasmid from this reference contains an H3-
469 G102A mutation, which was corrected to the WT G102. H3C110 was mutated to alanine and
470 H3H113 was mutated to alanine, asparagine or tyrosine. pBL105 and pBL108 plasmids for
471 *Saccaromyces cerevisiae* H3 and H4, respectively, were kindly provided by Bing Li, PhD, UT

472 Southwestern Medical Center. H3A110 was mutated to cysteine and H3H113 was mutated to
473 alanine, asparagine or tyrosine.
474
475 **Preparation of solutions and glassware.** All glassware was treated with 3.7% hydrochloric acid
476 for 12 hours followed in some cases by 12 hours of 10% nitric acid to remove trace metal
477 contamination. All solutions, buffers, and washes were prepared using Nanopure Diamond
478 (Thermo Fisher) ultra-pure water. Solutions were prepared using Bioultra grade reagents and
479 remaining trace metals removed with Chelex 100 (Sigma). Standard RC dialysis tubing for dialysis
480 (Spectrumlabs.com) was washed twice in 10 mM EDTA (99.99% trace metal basis – Sigma) at
481 80°C and cooled to room temperature for 16 hours. For yeast media, addition of all components
482 was done without the use of metal spatulas. Media was filtered through 0.2 μm membranes.
483 Fermentative media was either YPD (1% Yeast Extract, 2% Peptone, 2% glucose), SC (synthetic
484 complete medium with 2% glucose, all amino acids, and uracil and adenine), SC lacking lysine,
485 or minimal medium (with 2% glucose and only the auxotrophic metabolites His, Leu, Met, and
486 uracil). Non-fermentative media was YPEG (1% Yeast Extract, 2% Peptone, 3% ethanol, 3%
487 glycerol). Agar media was prepared similarly using acid-washed glassware. Agar media for
488 hypoxic growth were supplemented with 20 μg/ml ergosterol, 0.5% Tween-80 and 0.5% ethanol.
489
490 **Histone purification.** Histone purification was performed as previously described (Luger et al.,
491 1999), except that purification by size exclusion was omitted and the solubilized inclusion bodies
492 were pre-cleaned by passage over a Hi-Trap Q-Sepharose column (GE healthcare) before loading
493 onto a Hi-Trap SP-Sepharose column (GE healthcare). Histones were eluted by a salt gradient from
494 200 mM to 600 mM NaCl, as described previously (Luger et al., 1999), and fractions containing

495 pure histones were pooled, dialyzed three times against 4 L of 2 mM β-mercaptoethanol (Sigma)
496 in water, flash frozen and lyophilized.
497
498 **Tetramer assembly.** H3-H4 tetramer assembly was performed as previously described (Luger et
499 al., 1999) with some adjustments. Briefly, equimolar amounts of H3 and H4 were dissolved in 7
500 M Guanidinium HCl, 20 mM Tris-HCl pH 7.5 and 10 mM DTT at a concentration of 1-2 mg/mL
501 total protein. Refolding was achieved by 1-2 hr dialysis at 4°C against 1 L of 2 M NaCl, 10 mM
502 Tris-HCl pH 7.5, 1 mM EDTA, 5 mM β-mercaptoethanol (T.E.B.), then 1-2 hr against 1 L of 1 M
503 NaCl, T.E.B., followed by 16 hrs against 0.5 M NaCl, T.E.B., except for *S. cerevisiae* H3-H4
504 tetramers used for Figure 3A, for which all dialysis steps were performed in 2 M NaCl T.E.B.. The
505 refolded tetramer was centrifuged for 5 min at 13000 rcf at 4°C to eliminate any insoluble particles
506 and purified by size exclusion chromatography on a HiLoad 16/600 Superdex 200 column (GE
507 healthcare) at 1 mL/min in 500mM NaCl, 1 mM Tris-HCl pH7.5. Fractions containing the tetramer
508 were concentrated using Amicon Ultra–15/Ultracel-10K centrifugal filters (Millipore). The flow-
509 through buffer was used as negative control ("buffer") in the copper reductase assay.
510
511 ***In vitro* copper reductase assay.** H3-H4 tetramer, or the same volume of control buffer, was
512 resuspended to a final concentration of 1 μM in 100 mM NaCl, 1 mM Neocuproine (Sigma) and
513 30 μM BioUltra TCEP (Sigma) pH 7.5. The reaction was started by adding a mix of $CuCl_2$ and
514 Tricine-HCl, pH 7.5, at final concentrations of 0.0125-0.5 mM and 0.125-5 mM, respectively.
515 Special care was taken to keep the ratio of $CuCl_2$: Neocuproine at 1:2 for all reactions. $CuCl_2$
516 reduction using NADPH (Sigma, Roche) as the electron donor was performed using a final
517 concentration of H3-H4 tetramer of 5.8 μM in 150 mM NaOAc pH 7.5, 33 mM NaCl, 1 mM

518 Neocuproine, 10 μM NADPH and started by the addition of 0.5 mM $CuCl_2$ / 7.5 mM Tricine-HCl,
519 pH 7.5. To reduce a solution of 0.5 mM Cu^{2+}-N-(2-Acetamido)iminodiacetic acid (ADA) (Sigma),
520 5 uM of H3-H4 tetramer were resuspended in 100 mM NaCl, 0.5 mM bicinchoninic acid (BCA)
521 (Sigma) and 100 μM TCEP. The reaction was started by addition of the substrate. Reduction of 0.5
522 mM Cu^{2+}-Nitrilotriacetic acid (NTA) (Sigma) was performed similarly, except for the addition of
523 200 μM NADH (Roche) as electron donor instead of TCEP. Absorbance at 448 nm (Neocuproine)
524 or 562 nm (BCA) was measured every 0.5 seconds using a Hewlett-Packard HP8453 diode-array
525 UV/Visible spectrophotometer. Standard curves for each condition were produced using 2 mM β-
526 Mercaptoethanol to ensure complete reduction of Cu^{2+}. Linearity of detection was verified and the
527 resulting parameters used to convert the absorbance units into Cu^{1+} molarity.
528
529 **Proteinase K treatment of tetramer.** Proteinase K (Sigma Aldrich) was dissolved in water at
530 20mg/mL and buffer exchanged into water using Zeba Spin desalting columns (Thermo Fisher
531 Scientific) to clean the enzyme from impurities. 200 μL of 1 μM tetramer or histone H3 reaction
532 mix was incubated with 100 ng of clean Proteinase K for 15 minutes at room temperature before
533 starting the *in vitro* copper reductase assay described above.
534
535 **N-Ethylmaleimide (NEM) treatment of tetramer.** 10 μM *Xenopus laevis* tetramer was incubated
536 with 1 mM NEM in 10 mM Tris-HCl pH 7.5, 500 mM NaCl for 30 min at room temperature.
537 NEM-treated and untreated tetramers were buffer exchanged into 1 mM Tris-HCl pH 7.5, 500 mM
538 NaCl using Zeba Spin desalting columns, concentrated in Amicon Ultra Centrifugal Filters
539 (Millipore) and reacted in the *in vitro* copper reductase assay described above.
540

541 **UV/visible Spectrophotometry.** Control buffer of each tetramer was used to zero background
542 absorption. The UV/visible spectra of 50 μM *X. laevis* H3-H4 tetramer in 500 mM NaCl and 5
543 mM Tris-HCl pH 7.5 was acquired first without addition of Cu^{2+}. This was followed by addition
544 of 0.25 or 0.5 molar equivalents of $CuSO_4$-Tricine pH 7.5 at a ratio of 1:10. The UV/visible spectra
545 of 500 μM *S. cerevisiae* H3-H4 tetramer in 2 M NaCl and 5 mM Tris-HCl pH 7.5 were analyzed
546 in the same manner. The same analysis was performed with the control buffer in the absence of the
547 tetramer and used as "buffer control". The Hewlett-Packard HP8453 diode-array UV/Visible
548 spectrophotometer was used for all measurements.
549
550 **Immobilized Metal Affinity Chromatography (IMAC).** IMAC HiTrap HP (GE Healthcare)
551 columns were washed with 10 column volumes (CV) of water before loading with 5 CV of 5 mM
552 $CuCl_2$. Unbound $CuCl_2$ was washed off with 10 CV water and the column was equilibrated with
553 10 CV of Binding Buffer (20 mM Imidazole, 1 mM Tris-HCl pH 7.5, 500 mM NaCl). 325-360 μg
554 of Tetramer in 1 mM Tris-HCl pH 7.5, 500 mM NaCl were loaded twice and washed with 10 CV
555 Binding Buffer followed by 10 CV Binding Buffer containing 100 mM imidazole. Elution was
556 performed using a 100-300 mM imidazole gradient for *S. cerevisiae* tetramers and a 20-1000 mM
557 imidazole gradient for *X. laevis* tetramers over 10 CV. Tetramer background binding to the
558 unloaded IMAC HiTrap HP was competed off with Binding Buffer containing 100 mM imidazole.
559
560 **Liquid culture growth curves.** Population doubling times were calculated from cells growing
561 exponentially in YPD or SC media. Total population doublings were calculated by measuring cell
562 densities (OD_{600}) in indicated media after up to 48 hours of incubation. For experiments involving

563 potassium cyanide treatment, cells from dense starter cultures were washed twice with 5 mM
564 EDTA pH 8 and once with water just before growth.
565
566 **Spot tests.** Cells from exponentially-growing cultures were 10-fold serially diluted and 5 µL of
567 cells were spotted on media plates as indicated in the figures. For experiments with the *H113N*
568 mutation in a single copy of the histone H3 gene, cells were washed twice with 5 mM EDTA pH
569 8 prior to spotting. Cells were incubated at 30°C for up to 7 days and imaged daily. Because of
570 differing growth rates in the various media conditions, images shown in the figures were captured
571 when sufficient growth had occurred and growth differences could be assessed, and this ranged
572 between 2-7 days. Experiments in hypoxic conditions were done using a 2.5 L sealable jar and
573 anaerobic gas generating sachets (AnaeroGen) designed to generate a hypoxic environment
574 (oxygen of <1%). 5-fold serially diluted cells were spotted on agar plates. Media for normoxic and
575 hypoxic conditions was supplemented with ergosterol and Tween-80 to support growth in low-
576 oxygen condition and sealed in the hypoxic jar for 7 days at 30°C before capturing images. For
577 plasmid shuffle spot tests, cells growing in SG medium lacking only tryptophan were 5-fold
578 serially diluted, and spotted on media containing 1 mg/mL 5-Fluoroorotic acid. Cells that survive
579 have lost pRM102, but maintain pRM200.
580
581 **Micrococcal nuclease (MNase) digestion.** MNase digestion was performed similarly to methods
582 described previously (Rando, 2010). Cells were grown in SC medium at 30°C for ~2 doublings,
583 fixed with 2% formaldehyde for 30 min at 30°C followed by glycine addition to quench
584 formaldehyde reactivity. $2x10^9$ cells were transferred to new tubes and resuspended in Zymolyase
585 buffer (1 M Sorbitol, 50 mM Tris pH 7.5, 10 mM β-mercaptoethanol) on ice. To initiate cell wall

586 digestion, 2 mg of Zymolyase 100-T was added and cells were incubated at 30°C for 35 min.
587 Spheroplasts were resuspended in MNase digestion buffer (1 M sorbitol, 50 mM NaCl, 10 mM
588 Tris pH 7.5, 5 mM $MgCl_2$, 1 mM $CaCl_2$, 500 μM spermidine, 0.075% Igepal CA-630, 10 mM
589 BME) and varying amounts of MNase (Sigma) were added. Samples were incubated at 37°C for
590 20 min before inactivation of MNase by 5X stop solution (5% SDS, 50 mM EDTA). Proteins were
591 then digested by proteinase K (Sigma), and formaldehyde crosslinks reversed, by incubation at
592 65°C for ~12 hrs. DNA was purified by standard phenol-chloroform extraction methods and
593 isopropanol precipitation. MNase-digested DNA samples were treated with RNase A (Roche) for
594 1 hr at 37°C. DNA samples were then purified using the Wizard SV PCR purification kit (Promega)
595 according to the manufacturer's protocol.
596
597 **MNase accessibility analysis.** MNase-digested DNA samples were normalized by concentration,
598 and visualized using the DNA ScreenTape assay on the TapeStation 2200 instrument (Agilent),
599 according to the manufacturer's protocol. Gel images exported with TapeStation Analysis software
600 (Agilent) were analyized using FIJI (ImageJ 1.48k). ScreenTape images shown and quantified are
601 representative examples of three replicate MNase digestions from separately grown cultures of the
602 same cell clones.
603
604 **Sample preparation for inductively-coupled plasma mass spectrometry (ICP-MS).** Cells from
605 overnight cultures in SC or YPD media were diluted to OD_{600} = 0.2-0.4 and grown at 30°C for ~3
606 doublings, or for 18 and 24 hrs in YPEG and SC-lys, respectively. Cells (4-12 x 10^8) were
607 collected, and washed twice in 1 mM EDTA to remove cell surface-associated metals and once in
608 water. Cell pellets were stored at -20°C for 1-3 weeks prior to preparation for ICP-MS. Plastic

609 bottles and cylinders used for preparation of solutions for sample digestion were treated with 7-
610 10% ACS grade nitric acid for 5 days at 50°C and rinsed thoroughly with water. Previously-stored
611 cell pellets were overlaid slowly with 70% Optima Grade nitric acid and digested at 65°C for 12-
612 16 hrs. Prior to mass spectrometry, the digested samples were diluted with water to a final
613 concentration of 2% nitric acid and a final volume of 3-5 mL.
614
615 **Inductively-coupled plasma mass spectrometry.** Total Fe and Cu content was measured by
616 inductively coupled plasma mass spectrometry on the Agilent 8800 ICP-QQQ in MS/MS mode.
617 The most abundant isotopes of iron and copper (i.e. Fe^{56} and Cu^{63}) were used to determine the total
618 cellular iron and copper levels. The metal content was determined using an environmental
619 calibration standard (Agilent 5183-4688), which contains 100x higher concentration of Fe
620 compared to Cu, which more accurately reflects biological samples. Every run was calibrated
621 individually, and ^{45}Sc or ^{89}Y were used as internal standards to compare the calibration with the
622 analyzed samples. All Cu and Fe measurements in our study were within the calibrated linear
623 ranges and above the lower limits of detection, as determined from multiple blank samples. ICP
624 MassHunter software was used for ICP-MS data analysis.
625
626 **RNA extraction.** For poly-A RNA sequencing analyses, cells were growing exponentially in SC
627 or YPD, or grown for 24 hrs in SC-lys at the time of harvesting. For RT-qPCR analyses, cells were
628 growing exponentially in YPD or were exposed to $CuSO_4$ for one hour in YPD at the time of
629 harvesting. In both cases, cells were collected by centrifugation and frozen at -20°C until further
630 processing. RNA was extracted using previously published methods (Schmitt et al., 1990). RNA
631 extracted for subsequent RNA-seq analysis are from two replicate experiments. The exceptions

632 are cells grown in SC which are from three replicates, and cells grown in SC-lys + 75 μM $CuSO_4$
633 which is from one experiment. RNA extracted for subsequent RT-PCR analysis are from four
634 replicate experiments.
635
636 **Sample preparation for poly-A RNA sequencing.** Prior to preparing RNA-seq libraries for
637 Illumina HiSeq sequencing, contaminating DNA was digested using Turbo DNase (Thermo
638 Fisher). RNA quality was then assessed using the RNA ScreenTape assay on the TapeStation 2200
639 instrument (Agilent), according to the manufacturer's protocol. Using TapeStation Analysis
640 software (Agilent), RNA Integrity Number equivalent (RINe) scores were calculated. Only
641 samples with RINe scores greater than 9 (out of 10) were used for sequencing library preparation.
642 RNA-sequencing libraries were then prepared either manually with the KAPA Stranded mRNA-
643 seq library prep kit (KAPA Biosystems), or with automation, using the Illumina TruSeq Stranded
644 mRNA Library Kit for NeoPrep (Illumina). For both approaches, libraries were prepared according
645 to the manufacturer's protocols. RNA-seq libraries were assessed for correct fragment size and the
646 presence of adapter dimers, using the DNA ScreenTape assay on the TapeStation 2200 instrument
647 (Agilent). Average library sizes of ~270 bp were observed and deemed correct. Libraries were
648 pooled for multiplexed sequencing and further purified using Agencourt RNAClean XP beads.
649 Total DNA concentration was adjusted to 10 nM for Illumina sequencing.
650
651 **mRNA-sequencing and data processing.** High throughput sequencing was performed on
652 Illumina's HiSeq 4000 system, with single-end 50 bp insert reads, and dedicated index reads. Total
653 read count per library ranged from ~1.5-9 million. De-multiplexed reads, in FASTQ file format,
654 were aligned to the R64-1-1 S288C reference genome assembly (sacCer3), which was downloaded

655 from the UCSC database, using Tophat 2.0.9 (Kim et al., 2013). The "-g 1" parameter was used to
656 limit the number of alignments for each read to one, the top-scoring alignment.
657
658 **Gene expression analysis.** Gene expression values, in reads per kilobase per million mapped reads
659 (RPKMs), for 6692 annotated open reading frames were calculated using SAMMate 2.7.4 (Xu et
660 al., 2011). Many of the 6692 annotated ORFs are labeled as "dubious" or "putative" in the
661 Saccharomyces Genome Database (SGD). They break down as follows: Dubious open reading
662 frame unlikely to encode a functional protein – 717; Putative protein of unknown function – 316;
663 Retrotransposon TYA Gag and TYB Pol genes – 90; Protein of unknown function – 141;
664 Pseudogenic fragment – 4; Other - 20. These 1288 annotated ORFs typically have low expression
665 values and were filtered out of the final analyses. The remaining 5404 ORFs were used for
666 comparisons between groups.
667
668 **RNA-sequencing gene sets.** Gene sets (e.g. Figure 6 – figure supplement 3D) were constructed
669 by downloading and merging gene ontology term gene lists from AmiGO 2 in March 2017. The
670 "copper homeostasis" and "iron homeostasis" gene sets were further modified by adding or
671 removing genes based on literature review.
672
673 **RT-qPCR.** Extracted nucleic acids were treated with Turbo DNase (Thermo Fisher) and further
674 purified with TRIzol (Thermo Fisher). Poly-A RNA was isolated using Dynabead oligo dT_{25}
675 magnetic beads (Thermo Fisher) and quantified using the Qubit RNA HS assay kit (Thermo
676 Fisher). Equal amounts of mRNA from the different samples were then used to synthesize cDNA,
677 with random hexamers as primers, using the SuperScript IV first-strand synthesis system (Thermo

678 Fisher). Five percent of each cDNA reaction was used in qPCR reactions prepared with the
679 PowerUP SYBR Green Master Mix (Thermo Fisher) and run on a Stratagene Mx3000P qPCR
680 instrument (Agilent). Primer pairs were designed to amplify regions of the Mac1 targets FRE7,
681 CTR1, IRC7, FRE1, and REE1 (Gross et al., 2000), and the loading control ACT1. Fold changes
682 were based on C_t values, normalized to ACT1, and calculated relative to the mean of WT in YPD.
683

684 **Oxygen consumption assay.** Oxygen consumption rates were measured in whole cells using the
685 Fiber Optic Oxygen Monitor, Model 110 (Instech laboratories Inc., Plymouth Meeting, PA). For
686 experiments in Figure 6A and B, cells growing exponentially in YPD or SC were diluted in either
687 YPEG or SCEG + 60 μM BCS, respectively, with or without additional $CuSO_4$, and incubated for
688 18-24 hrs. Cells were diluted sufficiently in YPEG such that final cell density in respiratory media
689 was less than OD_{600} = 3. For experiments in Figure 6C, cells were diluted to OD_{600} = 1 in YPEG
690 with or without additional $CuSO_4$ and incubated for 4 hrs. Note that no growth had occurred in
691 that time period due to the respiratory deficiency of *ctr1Δ* strains. For experiments in Figure 8,
692 cells were diluted in YPEG with or without BCS and grown at 30°C for 12 hrs. For experiments
693 involving Antimycin A treatment in YPEG, cells were incubated for 6 hrs in the presence of
694 antimycin. Cells were collected by centrifugation and pellets concentrated in fresh media for the
695 oxygen consumption measurements. Consumption was recorded for 5 minutes and the rate was
696 determined for a one-minute linear consumption period.
697

698 **Mitochondrial DNA quantification.** Cells grown as described above for oxygen consumption
699 experiments were collected by centrifugation and lysed by bead beating in Lysis buffer 1 (100 mM
700 NaCl, 1 mM EDTA, 10 mM Tris pH 8). Lysates were then treated with RNase A (Sigma) at 37°C

701 1 hr in Lysis buffer 2 (Lysis buffer 1 with 0.5% Triton X-100) and subsequently with proteinase K
702 (Sigma) at 56°C for 2 hrs in Lysis buffer 3 (Lysis buffer 1 with 2% Triton X-100 and 1% SDS).
703 DNA was purified by standard phenol-chloroform extraction methods and ethanol precipitation.
704 0.1 ng of total DNA was used in qPCR reactions prepared with the PowerUP SYBR Green Master
705 Mix (Thermo Fisher) and run on a Stratagene Mx3000P qPCR instrument (Agilent). Primer pairs
706 were designed to amplify regions of the COX3 gene on the mitochondrial genome, and ACT1 on
707 the nuclear genome. Mitochondrial DNA (mtDNA) copy numbers were estimated based on C_t
708 values compared to ACT1. Oxygen consumption rates were scaled by the relative difference in
709 mtDNA content.
710
711 **Cytochrome *c* Oxidase assay.** Cells growing exponentially in YPD were diluted to OD_{600} = 1 in
712 YPEG with or without additional $CuSO_4$ and incubated for 4 hrs. Note that no growth had occurred
713 in that time period due to the respiratory deficiency of *ctr1Δ* strains. A mitochondria-enriched
714 subcellular fraction was then prepared from ~$2x10^9$ cells using methods described previously
715 (Gregg et al., 2009), with some modifications. Prior to spheroplasting, cells were washed once
716 with 1 mM EDTA, once with water. Cell wall digestion was accomplished using Zymolyase 100-
717 T (Nacalai Tesque) for 35 min at 30°C. The crude mitochondrial fraction was resuspended in 60
718 µL of Enzyme buffer (10 mM Tris/HCl pH 7, 250 mM sucrose, 0.5% Tween 20). Cytochrome c
719 oxidase activity was assessed similarly to a method described previously (Spinazzi et al., 2012). 1
720 mM Cytochrome *c* (from equine heart, Sigma) was reduced by addition of 1 mM sodium
721 hydrosulfite. Full reduction was confirmed by the ratio of absorbance at 550 nm to 565 nm being
722 greater than 10. Reactions were carried out in 100 µL volumes at 30°C with 85 µL of Assay buffer
723 (10 mM Tris/HCl ph 7, 120 mM KCl), 5 µL of reduced cytochrome c (50 µM) and 10 µL of

724 mitochondria-enriched samples at a final concentration of 20 – 50 µg/mL. Cytochrome c oxidation
725 was assessed by measuring absorbance at 550 nm over the course of 5 min using a Hewlett-Packard
726 HP8453 diode-array UV/Visible spectrophotometer, and the rate was determined for a one-minute
727 linear oxidation period.
728
729 **Sample preparation for Sod1 assays.** Sod1p superoxide dismutase activity was assayed by
730 native-PAGE and in-gel staining with nitrotetrazolium blue (NBT), and the Sod1p disulfide bond
731 was assayed by IAA labeling of thiols and gel mobility shift, based on previously-reported
732 methodology (Leitch et al., 2009). For WT and *ctr1Δ* strains (Figure 7A and B), ~$4x10^8$
733 exponentially growing cells in SC with or without supplemental $CuSO_4$ were collected and
734 resuspended in Lysis Buffer (600 mM sorbitol, 10 mM HEPES pH 7.5, 5 mM EDTA and protease
735 inhibitors) containing 1 mM iodoacetamide (IAA) (Figure 7B only). The lysate was split in two
736 for Sod1 activity assays and assessment of the Sod1 disulfide bond. For *ccs1Δ* strains (Figure 7D),
737 following an overnight growth in SC, cells were diluted to OD_{600} = 1 in minimal media with the
738 indicated amounts of $CuSO_4$. Cells were incubated at 30°C for 2 hrs, at which point ~$2x10^9$ cells
739 were collected and resuspended in Lysis Buffer. Cells were lysed with glass beads. Lysates were
740 prepared for both native-PAGE and SDS-PAGE with either native sample buffer (12.5% glycerol,
741 31.25 mM Tris pH 6.8, 0.005% bromophenol blue, 5 mM EDTA final concentrations) or SDS
742 sample buffer (5% glycerol, 40 mM Tris pH 6.8, 1% SDS, 0.005% bromophenol blue) with (Sod1p
743 content) or without (disulfide bond) 50 mM DTT, respectively.
744
745 **In-gel Sod1 activity assay.** For native-PAGE, ~10 µg (WT, $H3^{H113N}$, and $H3^{H113Y}$), ~20 µg (*ctr1Δ*
746 and $H3^{H113N}$*ctr1Δ*) or ~100 µg (*ccs1Δ* and $H3^{H113N}$*ccs1Δ*) of total protein was run on a 10%

747 acrylamide gel for 2.5 hrs with 1 mM EDTA in the running buffer. Gels were then sequentially
748 incubated in phosphate buffer (50 mM K_2HPO_4 pH 7.8, 1 mM EDTA), 0.48 mM NBT (Sigma) in
749 phosphate buffer, and 30 μM riboflavin (Sigma) and 0.02% Tetramethylethylenediamine
750 (TEMED; ThermoFisher) in phosphate buffer at room temperature. Finally, gels were exposed to
751 bright light and scanned using an Epson document scanner. Signal intensities of the major SOD1
752 band were then quantified using FIJI (ImageJ 1.48k). For the analysis in Figure 7 – figure
753 supplement 1A, signal intensities from four separate gels were normalized based on the average
754 signal intensity in each gel. Relative signal intensities, compared to the WT sample, were then
755 calculated based on the normalized intensities.
756
757 **Sod1p Western Blotting and Sod1 internal disulfide bond measurement.** For western blots to
758 determine Sod1p content, 10 μg of total protein content was run on 10% SDS acrylamide gels.
759 Western blots were performed using a primary antibody against Sod1p, a gift from Valeria Culotta
760 (JH764) (Leitch et al., 2009). The antibody was diluted 1:5000 in Odyssey blocking buffer (LI-
761 COR biotechnology) and blots were incubated at room temperature for 1.5 hrs. Signal
762 quantifications were obtained using the Odyssey infrared fluorescence imaging system (LI-COR
763 biotechnology) and Image Studio Lite software. For western blots to determine the amount of
764 disulfide bond, 10 μg (WT, $H3^{H113N}$, and $H3^{H113Y}$) or 15 μg (*ctr1Δ* and $H3^{H113N}$*ctr1Δ*) of total
765 protein content was run on 18% SDS acrylamide gels. After electrophoresis, gels were incubated
766 for 45 min with SDS running buffer containing 5% β-mercaptoethanol at room temperature.
767 Western blotting for Sod1p, and signal quantification were performed as described above, except
768 the primary antibody was diluted 1:2500.
769

770 **SDS-PAGE and Western Blotting for histone content.** For assessment of histone protein
771 content, whole cell protein extracts were prepared from $5x10^8$ cells growing exponentially in YPD.
772 Cell pellets were resuspended in 0.2 M NaOH and incubated at room temperature for 15 minutes.
773 Cells were then pelleted and resuspended in SDS-PAGE loading buffer (50 mM Tris-HCl pH 6.8,
774 2% SDS, 10% glycerol, 1% β-mercaptoethanol) and boiled for 5 minutes. For western blots, 4 µg
775 of total protein was run on 15% SDS acrylamide gels. Primary antibodies to histone H3 (Active
776 Motif, 39163) and H4 (Abcam, 10158) were diluted in Odyssey blocking buffer (LI-COR
777 biotechnology) at 1:5000 and 1:800, respectively, and blots were incubated in diluted antibody at
778 4°C overnight. Signal quantification was performed as described above.
779
780 **Statistical analyses.** The number of experimental replicates (n), and the observed significance
781 levels are indicated in figure legends. All statistical analyses were performed using Graphpad
782 Prism 5 or 7, unless otherwise stated. Significance values for pair-wise comparisons of doubling
783 times were calculated using the Mann-Whitney test. Significance values for comparisons of the
784 oxygen consumption rates in Figure 6 – figure supplement 1A were calculated using the Holm-
785 Sidak method for multiple t-tests, with alpha = 0.05. Significance values for pair-wise comparisons
786 of population doublings in Figure 6 – figure supplement 1B, oxygen consumption rates in Figures
787 6A-C and 8D, cytochrome *c* oxidase activity in Figure 6D, culture densities in Figures 6H, 7E, 8B,
788 and 8C, relative Sod1 activity assay signal intensities in Figure 7 – figure supplement 1A, and gene
789 expression fold changes in Figure 5C were calculated using unpaired Welch's t-test. Significance
790 values for comparisons of culture densities in Figures 8E and F were calculated using a mixed
791 model Two-Way ANOVA with Bonferroni post-hoc test for pair-wise comparisons. Statistical
792 testing for iron and copper measurements was done using unpaired Student's t-tests. For gene

793 expression data, we averaged RPKM values from replicates and used mean values for calculation
794 of global gene expression correlations (e.g. Figure 5 – figure supplement 1) and for analyzing gene
795 sets (e.g. Figure 6 – figure supplement 3D). For global correlations, Spearman's rank correlation
796 coefficients were calculated. Significance values for pair-wise comparisons of gene expression
797 levels of gene sets (e.g. Figure 6 – figure supplement 3D) were calculated using the Mann-Whitney
798 test. We also assessed differential gene expression, using the SAMMate RPKM values, for each
799 gene and between WT and $H3^{H113N}$ strains grown in SC media. Student's t-test was used to
800 calculate p values with the Benjamini-Hochberg procedure to control the false discovery rate at
801 0.1. Curve fitting for enzymatic kinetic analysis was performed online using "mycurvefit" tool
802 (https://mycurvefit.com),. Predicted values for 0.03 or 0.05 seconds were within 20% of the
803 maximum values detected and used to calculate the initial velocities, which were then transferred
804 to Graphpad Prism version 5.01 and fitted with the Michaelis-Menten non-linear regression
805 function to determine enzymatic parameters.
806
807 **Data availability**
808 Gene expression datasets generated by mRNA-sequencing experiments have been deposited in the
809 NCBI GEO database under the primary accession number GSE100034.
810

Acknowledgements

We thank Heather Christofk for useful discussions, Mayo Thompson for proofreading, Marco Morselli for assistance in RNA-seq library preparation, Valeria Culotta for the α-SOD1 antibody and helpful guidance in Sod1 assays, and the UCLA Broad Stem Cell Center Sequencing Core. This work was supported in part by a W. M. Keck Foundation Award to S.K.K. and S.S.M. and NIH grants CA178415 to S.K.K., GM074701 to M.F.C., GM42143 to S.S.M., and CA188592 to M.V. O.A.C was supported by the Whitcome and O.A.C. and C.C. by the Dissertation Year Fellowships from UCLA. N.A. was supported by the NCI Ruth L. Kirschstein NRSA for Individual MD/PhD Degree Fellows F30 CA186619 and NIH training grant T32 GM8042. S.Z. was supported by the Amgen Scholars Program.

Author contributions

Conceptualization, N.A., O.A.C., M.V., Y.X., and S.K.K.; Methodology, N.A., O.A.C., M.V., Y.X., M.F.C., S.S.M., and S.K.K.; Investigation, N.A., O.A.C., M.V., Y.X., C.C., S.S., L.Y., N.M., S.Y., S.Z., J.D., and S.K.K.; Formal Analysis, N.A., O.A.C., and M.V.; Writing – Original Draft, N.A., O.A.C., M.V., and S.K.K.; Writing – Review & Editing, N.A., O.A.C., M.V., Y.X., L.Y., S.S., M.F.C., S.S.M. and S.K.K.; Resources, N.A., O.A.C., M.V., C.C., L.Y., M.F.C., S.S.M., and S.K.K.; Visualization, N.A., O.A.C., and M.V.; Supervision, S.K.K.; Project Administration, S.K.K.; Funding Acquisition, M.F.C., S.S.M., and S.K.K.

Competing interests

The authors declare no competing interests.

833 **Figure Legends**

834

835 **Figure 1. Recombinant histone H3-H4 tetramer interacts with cupric ions**.

836 **(A)** *Left*: *X. laevis* nucleosome core particle structure (PDB:1KX5) (Davey et al., 2002) viewed
837 down the DNA superhelix axis. Histones H3, H4, H2A and H2B are shown in metallic orange,
838 blue, green and red, respectively. The square box delineates the H3-H3' interface. *Right*: Interface
839 residues H113 and C110, one from each of the histone H3 proteins, are highlighted. **(B)** Alignment
840 of the C-terminal region of *S. cerevisiae* histone H3, human non-centromeric histone H3 variants,
841 and M. *fervidus* HMf-1 and HMf-2. **(C)** *Left panel*: UV-vis absorbance spectrum of the *X. laevis*
842 H3-H4 tetramer incubated with increasing molar equivalents of Cu^{2+}. Inset: Differential UV
843 absorbance compared to the absorbance of the tetramer alone, and without subtraction of buffer
844 absorbance. *Right panel*: Buffer-corrected differential UV absorbance at 245nm of the indicated
845 *X. laevis* tetramers incubated with increasing molar equivalents of Cu^{2+}. **(D)** Elution of the
846 indicated *X. laevis* tetramers from a Cu^{2+}-IMAC column. *Left panel*: Image of coomassie stained
847 PAGE of input (25%), flow-through, and fractions eluted at indicated concentrations of imidazole.
848 *Right panel*: corresponding FPLC elution profile over a gradient of increasing imidazole
849 concentrations. Peaks of tetramers appear over background absorbance of increasing imidazole
850 concentrations (i.e., lines trending up).

851

852 **Figure 2. The *Xenopus laevis* H3-H4 tetramer is a copper reductase**.

853 **(A)** Photographic representation of *in vitro* copper reductase assay at indicated times. Control
854 buffer or *X. laevis* tetramer were reacted with 30 μM TCEP and 1 mM $CuCl_2$ in 10 mM Tricine
855 pH 7.5 in presence of neocuproine (NC) Cu^{1+} chelator. The yellow color is due to NC_2-Cu^{1+}
856 complex formation. **(B)** Progress curves of copper reduction by 1 μM of *X. laevis* H3-H4 tetramer,

857 heat-inactivated tetramer, or buffer in presence of 30 μM TCEP and 1 mM $CuCl_2$ in 10 mM Tricine.
858 Lines and shading represent the mean ± SD of 3-5 assays. **(C)** Same as (B) using 1 μM of *X. laevis*
859 tetramer and equimolar monomeric *X. laevis* H3 before and after digestion with Proteinase K (PK).
860 **(D)** Same as (B) with indicated TCEP concentrations. **(E)** Same as (B) with indicated $CuCl_2$
861 concentrations. **(F)** Progress curves of copper reduction by 1 μM of *X. laevis* tetramer using 20
862 μM NADPH as the electron donor with 0.5 mM $CuCl_2$ in 7.5 mM Tricine pH 7.5. Lines and
863 shading represent the mean ± SD of 3-5 assays. **(G)** Same as (B) with the indicated *X. laevis*
864 tetramers. **(H)** Same as (B) with and without NEM treatment of the tetramer. **(I)** Progress curves
865 of copper reduction by 5 μM of the indicated *X. laevis* tetramers in presence of 100 μM TCEP and
866 0.5 mM $CuCl_2$ in 0.5 mM ADA pH 8.
867
868 **Figure 3. The *Saccharomyces cerevisiae* H3-H4 tetramer potentially is a copper reductase**.
869 **(A)** *Left panel*: Differential absorbance of visible light between 500 and 900 nm compared to the
870 absorbance of the yeast tetramer alone, and without subtraction of buffer absorbance. *Right panel*:
871 Buffer-corrected differential red light absorbance at 680 nm of the indicated yeast tetramers
872 incubated with increasing molar equivalents of Cu^{2+}. **(B)** Elution of the indicated *S. cerevisiae*
873 tetramers from a Cu^{2+}-IMAC column. *Left panel*: Image of coomassie stained PAGE of input
874 (25%), flow-through, and fractions eluted at indicated concentrations of imidazole. *Right panel*:
875 corresponding FPLC elution profile over a gradient of increasing imidazole concentrations. Peaks
876 of tetramers appear over background absorbance of increasing imidazole concentrations (i.e., lines
877 trending up). **(C)** Buffer-corrected differential UV absorbance at 245 nm of the indicated *S.*
878 *cerevisiae* tetramers incubated with increasing molar equivalents of Cu^{2+}. **(D)** Progress curves of
879 copper reduction by 5 μM of the indicated *S. cerevisiae* tetramers in presence of 100 μM TCEP
880 and 0.5 mM $CuCl_2$ in 0.5 mM ADA pH 8.

881 **Figure 4. Mutation of histone H3 histidine 113 in *S. cerevisiae* is a loss of function.**

882 **(A)** Plasmid shuffle assay with strains harboring WT H3 on a URA3 plasmid and the indicated H3
883 gene on a TRP1 plasmid. 5-Fluoro-orotic acid (5-FOA) is lethal to cells bearing the URA3 plasmid,
884 and therefore selects for cells that maintain only the indicated H3 plasmid. **(B)** Average doubling
885 times from steady-state growth in liquid Synthetic Complete (SC) medium. Bar graphs show mean
886 ± standard deviation (SD) from 3-9 replicate cultures. **(C)** Spot test assay in fermentative medium
887 (YPD). Note that the *HHT1* gene in the bottom three strains was placed under the control of the
888 *GAL1* promoter, which is repressed in YPD. Since one copy of *H3H113N* or *H3H113Y* (rows 7
889 and 8) causes a more severe phenotype than two copies ($H3^{H113N}$ and $H3^{H113Y}$, rows 4 and 5), this
890 suggests that they are likely loss of function mutations.

891

892 **Figure 5. Mutation of H3H113 decreases the copper-dependent repression of Mac1 target**
893 **genes.**

894 **(A)** Heat map of average fold changes of Mac1 target gene (Gross et al., 2000) expression, relative
895 to WT for each gene and normalized to ACT1 fold changes, based on mRNA-seq analyses from
896 two independent experiments. Genes have been ordered vertically based on the fold increase in the
897 $H3^{H113N}$*ctr1Δ* strain (4th column). Note that *CTR3* is a Mac1 target gene but is not expressed in
898 this strain background due to a genetic disruption by a Ty2 transposon. **(B)** Same as (A) except
899 showing fold changes in expression levels based on RT-qPCR analyses. The data are averages from
900 four independent experiments in fermentative medium (YPD). Genes have been ordered vertically
901 based on the fold increase in the $H3^{H113Y}$ strain. **(C)** Intracellular copper content measured by ICP-
902 MS for exponentially growing strains in YPD. Data are presented as mean ± SD from 3-6 replicate
903 cultures. **(D)** Fold changes in expression levels for two Mac1 target genes, normalized to ACT1,

904 based on RT-qPCR analyses. Mac1 activation was induced by deletion of *CTR1* and repressed by
905 1 hr treatment with $CuSO_4$ in YPD as indicated. Bars are the sample means and each dot is an
906 independent experiment (n = 4). *P≤0.05, **P≤0.01, ***P<0.001.
907
908 **Figure 6. The H3H113 residue is required for efficient use of copper for mitochondrial**
909 **respiration.**
910 **(A)** Oxygen consumption assays of cells incubated for 18 hrs in liquid YPEG. Baseline copper
911 concentration in YPEG is ~1 μM. Bars show means ± SD from three independent experiments
912 done concurrently with the same batch of media and scaled to relative mitochondrial DNA contents
913 (data not shown). **(B)** Same as (A) but with cells incubated in SCEG + 60 μM BCS. Baseline
914 copper concentration in SCEG is ~1 μM. **(C)** Oxygen consumption assays of cells incubated for 4
915 hrs in liquid YPEG with increasing amounts of $CuSO_4$. Bars show means in log_2 scale ± SD from
916 three independent experiments. **(D)** Cytochrome *c* oxidase assays of cells incubated for 4 hrs in
917 liquid YPEG with increasing amounts of $CuSO_4$. Bars show means in log_2 scale ± SD from three
918 independent experiments. N.D.: not detectable. **(E)** Spot test assays in fermentative (YPD) or
919 respiratory media (YPEG) with the indicated amounts of $CuSO_4$. **(F)** Same as (E). **(G)** Average
920 doubling times ± SD from steady-state growth in liquid YPD from three replicate cultures. **(H)**
921 Average OD_{600} ± SD for growth in liquid YPEG with increasing amounts of $CuSO_4$ after 36 hrs
922 from three replicate cultures. *P≤0.05, **P≤0.01, ***P<0.001.
923
924 **Figure 7. *H3^{H113N}* is deficient in utilizing copper for Sod1 activity and function.**
925 **(A)** Sod1 in-gel activity assay (top) and corresponding Sod1p western blot (bottom) for cells grown
926 in SC medium with the indicated amounts of additional $CuSO_4$. Baseline copper concentration in

927 SC medium is ~0.16 μM. Numbers are relative signal intensities for each pair of bands. Gel and
928 blot shown are representative of four independent experiments. **(B)** Same as (A), except paired
929 with an Sod1 disulfide bond assay (bottom). Numbers below the blot are relative amount of
930 oxidized Sod1 compared to the total Sod1 protein. Bands shown are representative of three
931 independent experiments. **(C)** Spot test assays on SC or SC-lys plates containing 1 mM and 10
932 μM BCS, respectively. **(D)** Same as (A) except for cells grown in minimal medium. Baseline
933 copper concentration in minimal medium is ~0.25 μM. Gel and blot shown are representative of
934 three independent experiments. **(E)** Growth assay in the indicated liquid media shown as mean
935 OD_{600} ± SD after 24 hrs from three independent experiments. **(F)** Same as (C). **P≤0.01,
936 ***P<0.001.
937
938 **Figure 8. The *H3A110C* mutation enhances copper utilization for respiratory growth in *S.***
939 ***cerevisiae*.**
940 **(A)** Spot test assays in fermentative (YPD) or respiratory media (YPEG). **(B)** Growth after 48 hrs
941 in liquid YPEG with increasing amounts of $CuSO_4$. Bars show mean OD_{600} ± SD from three
942 independent experiments done concurrently with the same batch of media. **(C)** Growth after 48 hrs
943 in liquid YPEG with increasing amounts of BCS. Bars show relative OD_{600} compared to the *gsh1Δ*
944 strain ± SD from three independent experiments. **(D)** Oxygen consumption assays of cells grown
945 in the indicated media for 12 hrs. Bar graphs show means ± SD of three independent experiments
946 done concurrently with the same batch of media and scaled to relative mitochondrial DNA contents
947 (data not shown). **(E)** Growth curves of the indicated strains in YPEG with potassium cyanide
948 (KCN) and increasing amounts of $CuSO_4$ in each panel, as indicated. Line graphs show means at
949 each time point ± SD from three independent experiments done concurrently with the same batch

950 of media. *** indicates significant (P≤0.001) difference at multiple time points. Note that minimal
951 growth occurred before 36 hrs. **(F)** Same as (E). **(G)** Spot test assays in YPD or YPEG with the
952 indicated amounts of $CuSO_4$. **(H)** Plasmid shuffle assay with strains harboring WT H3 on a URA3
953 plasmid and the indicated H3 gene on a TRP1 plasmid. 5-Fluoro-orotic acid (5-FOA) is lethal to
954 cells bearing the URA3 plasmid, and therefore selects for cells that maintain only the indicated H3
955 plasmid. *P<0.05, **P≤0.01, ***P≤0.001.
956
957 **Figure 1 – figure supplement 1. *In vitro* H3-H4 tetramer formation.**
958 **(A)** The procedure for preparation of histones and assembly of the *X. laevis* and yeast H3-H4
959 tetramer is outlined. **(B)** FPLC elution profiles of the indicated *X. laevis* tetramers. **(C)** Image of
960 coomassie-stained PAGE of the indicated purified *X. laevis* tetramers.
961
962 **Figure 2 – figure supplement 1. Graphical representation of the copper reductase assay.**
963
964 **Figure 2 – figure supplement 2. *In vitro* copper reductase assay with the *Xenopus laevis* H3-**
965 **H4 tetramer**.
966 **(A)** Standard curve for Cu^{1+} detection for copper reductase assay conditions used with *X. laevis*
967 tetramers with increasing amounts of $CuCl_2$-Tricine pH 7.5 at a ratio 1:10 in presence of 2 mM β-
968 Mercaptoethanol as reducing agent (see Methods). Error bars indicate mean ± SD of three replicate
969 measurements. **(B)** Same as (A) but for reactions with increasing amounts of $CuCl_2$-Tricine pH 7.5
970 at a ratio 1:15 (see Methods). **(C)** Progress curve of copper reduction using 30 μM TCEP as the
971 electron donor with 1 μM of *X. laevis* tetramer, equimolar monomeric *X. laevis* histone H3, and
972 equimolar monomeric *S. cerevisiae* histone H2A. **(D)** Henri-Michaelis-Menten curves of initial

973 velocities of reactions with the *X. laevis* tetramer. **(E)** Calculated enzymatic parameters of the
974 tetramer from the curve in (D). **(F)** Same as (C) but with *X. laevis* tetramer, or equimolar RNase A
975 or DTT. **(G)** Same as (A) but for reactions with increasing amounts of $CuCl_2$-ADA pH 8 at a ratio
976 1:1 (see Methods). **(H)** Same as (A) but for reactions with increasing amounts of $CuCl_2$-NTA pH
977 7.6 at a ratio 1:1 (see Methods). **(I)** Progress curves of copper reduction by 5 μM of the indicated
978 *X. laevis* tetramers in presence of 200 μM TCEP and 0.5 mM $CuCl_2$ in 0.5 mM NTA pH 7.6.
979
980 **Figure 3 – figure supplement 1. Assembly of *S. cerevisiae* WT and mutant H3-H4 tetramers.**
981 **(A)** Image of coomassie-stained PAGE of the indicated purified *S. cerevisiae* tetramers. **(B-D)**
982 FPLC elution profiles of the indicated *S. cerevisiae* tetramers. **(E)** Same as (A). **(F-G)** Same as
983 (B).
984
985 **Figure 5—figure supplement 1. Mutation of H3H113 does not result in global gene expression**
986 **changes.**
987 Scatterplots of average global gene expression values from exponentially growing cells in
988 fermentative media (SC, n=3 and YPD, n=2), with Spearman's rank correlation coefficients (r_s) as
989 indicated.
990
991 **Figure 6—figure supplement 1. The *H3H113N* mutation diminishes copper utilization for**
992 **mitochondrial respiration.**
993 **(A)** Bar graphs show mean oxygen consumption rates ± SD of the indicated strains from three
994 independent experiments after 6 hrs in liquid YPEG with indicated amount of $CuSO_4$ in presence
995 or absence of antimycin A, a mitochondrial complex III inhibitor. Note that cells were pre-loaded

996 with copper prior to growth in YPEG. **(B)** Growth during 48 hrs in liquid YPEG with increasing
997 amounts of $CuSO_4$. Bars show mean population doublings ± SD from three independent
998 experiments done concurrently with the same batch of media. **(C)** Spot test assays in fermentative
999 (YPD) or respiratory media (YPEG) with the indicated amounts of $CuSO_4$. Baseline copper
1000 concentration in YP media is ~1 μM. **(D)** Same as (C) except with the indicated amounts of
1001 $MnSO_4$, $ZnSO_4$, or $FeCl_3$. Note that the *ctr1*Δ strain is respiratory deficient and cannot be rescued
1002 by exogenous manganese, zinc or iron. *P≤0.05, ***P≤0.001.
1003
1004 **Figure 6—figure supplement 2. Decrease of the dosage of WT histone H3 and H4 genes.**
1005 **(A)** Western blots of histone H3 and H4 and coomassie-stained 15% SDS-PAGE, including the
1006 relative signal intensity for the indicated strains. **(B)** Signal intensity profiles from chromatin
1007 digested with 0.1 units of MNase. A.U.: arbitrary units.
1008
1009 **Figure 6—figure supplement 3. The *H3H113N* mutation does not significantly affect**
1010 **chromatin accessibility or gene expression in respiratory media.**
1011 **(A)** Quantitative representation of the signal intensity profiles (right) from chromatin digested with
1012 the indicated amounts of MNase (left) from exponentially growing cells in SC. A.U.: arbitrary
1013 units. **(B)** Spot test assays in fermentative (YPD) or respiratory media (YPEG) with the indicated
1014 amounts of $CuSO_4$. Baseline copper concentration in YP media is ~1 μM. **(C)** Scatterplot of
1015 average global gene expression values from exponentially growing cells in respiratory media
1016 (YPEG, n=2), with Spearman's rank correlation coefficients (r_s) as indicated. **(D)** Average mRNA
1017 expression levels for three gene sets comparing fermentative (YPD) and respiratory (YPEG)
1018 growth conditions from two independent experiments. Each dot is the average RPKM values for

1019 an individual gene within the sets and the central lines and whiskers represent the median and
1020 interquartile range. **(E)** Heat map of average mRNA expression levels for copper homeostasis
1021 genes (data summarized in panel D) from two independent experiments. Genes have been sub-
1022 grouped based on known functions of the gene products and ordered vertically within the groups
1023 based on the RPKM values of the WT strain in YPEG medium (3rd column). *P≤0.05, ***P≤0.001.
1024

1025 **Figure 6—figure supplement 4. Disruptions in copper utilization are not accounted for by**
1026 **changes in copper content or sequestration by Cup1.**

1027 **(A)** Intracellular copper (left) and iron (right) content of cells grown in the indicated media for 3-
1028 4 doublings for WT and *H3*^{H113N} and 12 hrs for *ctr1*Δ strains. Bar graphs represent mean ± SD from
1029 3-6 replicate cultures. #The *ctr1*Δ strains, which do not grow in non-fermentable media, were
1030 incubated in YPEG and assessed for metal content for reference. **(B)** Spot test assays in
1031 fermentative (YPD) or respiratory media (YPEG) with the indicated amounts of $CuSO_4$. Baseline
1032 copper concentration in YP media is ~1 μM. *P≤0.05.
1033

1034 **Figure 6—figure supplement 5. Disruption of cell surface metalloreductases or glutathione**
1035 **synthesis affect copper utilization differently than H3H113 mutations.**

1036 **(A-B)** Spot test assays in fermentative (YPD) or respiratory media (YPEG) with the indicated
1037 amounts of $CuSO_4$. Baseline copper concentration in YP media is ~1 μM.
1038
1039
1040

1041 **Figure 7—figure supplement 1. The *H3H113N* mutation diminishes copper utilization for**
1042 **Sod1 activity.**
1043 **(A)** Normalized relative signal intensities of Sod1 in-gel activity assays for cells grown in SC
1044 medium with the indicated amounts of additional $CuSO_4$ (representative gel image in Figure 7A).
1045 Bars are the sample means and each dot is an independent experiment (n = 4). Baseline copper
1046 concentration in SC medium is ~0.16 μM. **(B-C)** Spot test assays of the indicated strains in
1047 fermentative (SC) media with or without lysine and with the indicated amounts of $CuSO_4$. **(D)**
1048 Same as (B). Hypoxia was generated with an air-tight chamber and an anaerobic gas producing
1049 sachet. **(E)** Same as (B) except with the indicated amounts of $MnSO_4$, $ZnSO_4$, or $FeCl_3$. Note that
1050 *ccs1*Δ or *sod1*Δ renders cells auxotrophic for lysine and cannot be rescued by exogenous
1051 manganese, zinc or iron. **P≤0.01.
1052
1053 **Figure 7—figure supplement 2. Disruptions in copper dependent Sod1 function are not**
1054 **accounted for by changes in copper content, sequestration by Cup1, or gene expression.**
1055 **(A)** Spot test assays of the indicated strains in fermentative (SC) media with or without lysine and
1056 with the indicated amounts of $CuSO_4$. Baseline copper concentration in SC medium is ~0.16 μM.
1057 **(B)** Intracellular copper (left) and iron (right) content measured by ICP-MS for exponentially
1058 growing strains in SC. Data are presented as mean ± SD from 3-6 replicate cultures. **(C)**
1059 Intracellular copper and iron content of cells grown in the indicated media for 3-4 doublings for
1060 WT and $H3^{H113N}$ and 24 hrs for *ccs1*Δ strains. Bar graphs represent mean ± SD from 3-6 replicate
1061 cultures. [#]The *ccs1*Δ strains, which grow minimally in SC-lys media, were assessed for metal
1062 content for reference. **(D)** Scatterplots of average global gene expression values from exponentially
1063 growing cells in SC or SC-lys media from two independent experiments, with Spearman's rank

1064 correlation coefficient (r_s) as indicated. **(E)** Heat map of average mRNA expression levels for
1065 copper homeostasis genes (data summarized in panel F) from two independent experiments. Genes
1066 have been sub-grouped based on known functions of the gene products and ordered vertically
1067 within the groups based on the RPKM values of the *ccs1*Δ strain in SC-lys medium (5th column).
1068 **(F)** Average mRNA expression levels for three gene sets in cells growing exponentially in SC, SC-
1069 lys, or SC-lys + 75 μM $CuSO_4$ media after 24 hrs from two independent experiments (except n=1
1070 for SC-lys+Cu). *P<0.05.

1071 **References**

1072 Adamczyk, M., Poznanski, J., Kopera, E., and Bal, W. (2007). A zinc-finger like metal binding site
1073 in the nucleosome. FEBS Lett *581*, 1409-1416.

1074 Adkins, M.W., Howar, S.R., and Tyler, J.K. (2004). Chromatin disassembly mediated by the
1075 histone chaperone Asf1 is essential for transcriptional activation of the yeast PH05 and PH08
1076 genes. Mol Cell *14*, 657-666.

1077 Agez, M., Chen, J., Guerois, R., van Heijenoort, C., Thuret, J.Y., Mann, C., and Ochsenbein, F.
1078 (2007). Structure of the histone chaperone ASF1 bound to the histone H3 C-terminal helix and
1079 functional insights. Structure *15*, 191-199.

1080 Anbar, A.D. (2008). Oceans. Elements and evolution. Science *322*, 1481-1483.

1081 Bal, W., Lukszo, J., Jezowska-Bojczuk, M., and Kasprzak, K.S. (1995). Interactions of nickel(II)
1082 with histones. Stability and solution structure of complexes with CH3CO-Cys-Ala-Ile-His-NH2,
1083 a putative metal binding sequence of histone H3. Chem Res Toxicol *8*, 683-692.

1084 Brachmann, C.B., Davies, A., Cost, G.J., Caputo, E., Li, J.C., Hieter, P., and Boeke, J.D. (1998).
1085 Designer deletion strains derived from Saccharomyces cerevisiae S288C: a useful set of strains
1086 and plasmids for PCR-mediated gene disruption and other applications. Yeast *14*, 115-132.

1087 Burkhead, J.L., Ralle, M., Wilmarth, P., David, L., and Lutsenko, S. (2011). Elevated Copper
1088 Remodels Hepatic RNA Processing Machinery in the Mouse Model of Wilson's Disease. J Mol
1089 Biol *406*, 44-58.

1090 Dancis, A., Haile, D., Yuan, D.S., and Klausner, R.D. (1994). The Saccharomyces-Cerevisiae
1091 Copper Transport Protein (Ctr1p) - Biochemical, Characterization, Regulation by Copper, and
1092 Physiological-Role in Copper Uptake. J Biol Chem *269*, 25660-25667.

1093 Davey, C.A., Sargent, D.F., Luger, K., Maeder, A.W., and Richmond, T.J. (2002). Solvent mediated
1094 interactions in the structure of the nucleosome core particle at 1.9 angstrom resolution. J Mol Biol
1095 *319*, 1097-1113.

1096 Dyer, P.N., Edayathumangalam, R.S., White, C.L., Bao, Y., Chakravarthy, S., Muthurajan, U.M.,
1097 and Luger, K. (2004). Reconstitution of nucleosome core particles from recombinant histones and
1098 DNA. Methods in enzymology *375*, 23-44.

1099 Feinstein, D.L., and Moudrianakis, E.N. (1986). Thiol reactivity of histone H3 in soluble and
1100 DNA-associated histone complexes: evidence for allosteric and torsional regulation.
1101 Biochemistry-Us *25*, 8409-8418.

1102 Finney, J., Moon, H.J., Ronnebaum, T., Lantz, M., and Mure, M. (2014). Human copper-dependent
1103 amine oxidases. Arch Biochem Biophys *546*, 19-32.

1104 Forbes, S.A., Beare, D., Gunasekaran, P., Leung, K., Bindal, N., Boutselakis, H., Ding, M.J.,
1105 Bamford, S., Cole, C., Ward, S.*, et al.* (2015). COSMIC: exploring the world's knowledge of
1106 somatic mutations in human cancer. Nucleic Acids Res *43*, D805-D811.

1107 Freedman, J.H., Ciriolo, M.R., and Peisach, J. (1989). The Role of Glutathione in Copper-
1108 Metabolism and Toxicity. J Biol Chem *264*, 5598-5605.

1109 Furukawa, Y., Torres, A.S., and O'Halloran, T.V. (2004). Oxygen-induced maturation of SOD1: a
1110 key role for disulfide formation by the copper chaperone CCS. Embo J *23*, 2872-2881.

1111 Goldstein, A.L., and McCusker, J.H. (1999). Three new dominant drug resistance cassettes for
1112 gene disruption in Saccharomyces cerevisiae. Yeast *15*, 1541-1553.

1113 Graden, J.A., and Winge, D.R. (1997). Copper-mediated repression of the activation domain in the
1114 yeast Mac1p transcription factor. Proceedings of the National Academy of Sciences of the United
1115 States of America *94*, 5550-5555.

1116 Gregg, C., Kyryakov, P., and Titorenko, V.I. (2009). Purification of mitochondria from yeast cells.
1117 J Vis Exp, 1417.

1118 Gross, C., Kelleher, M., Iyer, V.R., Brown, P.O., and Winge, D.R. (2000). Identification of the
1119 copper regulon in Saccharomyces cerevisiae by DNA microarrays. J Biol Chem *275*, 32310-32316.

1120 Hassett, R., Dix, D.R., Eide, D.J., and Kosman, D.J. (2000). The Fe(II) permease Fet4p functions
1121 as a low affinity copper transporter and supports normal copper trafficking in Saccharomyces
1122 cerevisiae. Biochem J *351*, 477-484.

1123 Hassett, R., and Kosman, D.J. (1995). Evidence for Cu(II) Reduction as a Component of Copper
1124 Uptake by Saccharomyces-Cerevisiae. J Biol Chem *270*, 128-134.

1125 Henneman, B., van Emmerik, C., van Ingen, H., and Dame, R.T. (2018). Structure and function of
1126 archaeal histones. PLoS Genet *14*, e1007582.

1127 Huang, H.L., Maertens, A.M., Hyland, E.M., Dai, J.B.A., Norris, A., Boeke, J.D., and Bader, J.S.
1128 (2009). HistoneHits: A database for histone mutations and their phenotypes. Genome Res *19*, 674-
1129 681.

1130 Huster, D., Finegold, M.J., Morgan, C.T., Burkhead, J.L., Nixon, R., Vanderwerf, S.M., Gilliam,
1131 C.T., and Lutsenko, S. (2006). Consequences of copper accumulation in the livers of the Atp7b(-
1132 /-) (Wilson disease gene) knockout mice. Am J Pathol *168*, 423-434.

1133 Katz, A.K., Shimoni-Livny, L., Navon, O., Navon, N., Bock, C.W., and Glusker, J.P. (2003).
1134 Copper-binding motifs: Structural and theoretical aspects. Helv Chim Acta *86*, 1320-1338.

1135 Kim, D., Pertea, G., Trapnell, C., Pimentel, H., Kelley, R., and Salzberg, S.L. (2013). TopHat2:
1136 accurate alignment of transcriptomes in the presence of insertions, deletions and gene fusions.
1137 Genome Biol *14*, R36.

1138 Klink, T.A., Woycechowsky, K.J., Taylor, K.M., and Raines, R.T. (2000). Contribution of disulfide
1139 bonds to the conformational stability and catalytic activity of ribonuclease A. Eur J Biochem *267*,
1140 566-572.

1141 Krishnamoorthy, L., Cotruvo, J.A., Jr., Chan, J., Kaluarachchi, H., Muchenditsi, A., Pendyala, V.S.,
1142 Jia, S., Aron, A.T., Ackerman, C.M., Wal, M.N., *et al.* (2016). Copper regulates cyclic-AMP-
1143 dependent lipolysis. Nat Chem Biol *12*, 586-592.

1144 Lee, K.P., Baxter, H.J., Guillemette, J.G., Lawford, H.G., and Lewis, P.N. (1982). Structural
1145 studies on yeast nucleosomes. Can J Biochem *60*, 379-388.

1146 Leitch, J.M., Jensen, L.T., Bouldin, S.D., Outten, C.E., Hart, P.J., and Culotta, V.C. (2009).
1147 Activation of Cu,Zn-Superoxide Dismutase in the Absence of Oxygen and the Copper Chaperone
1148 CCS. J Biol Chem *284*, 21863-21871.

1149 Lin, S.J., and Culotta, V.C. (1996). Suppression of oxidative damage by Saccharomyces cerevisiae
1150 ATX2: Which encodes a manganese-trafficking protein that localizes to Golgi-like vesicles. Mol
1151 Cell Biol *16*, 6303-6312.

1152 Liu, J., Chakraborty, S., Hosseinzadeh, P., Yu, Y., Tian, S., Petrik, I., Bhagi, A., and Lu, Y. (2014).
1153 Metalloproteins containing cytochrome, iron-sulfur, or copper redox centers. Chem Rev *114*, 4366-
1154 4469.

1155 Longtine, M.S., McKenzie, A., Demarini, D.J., Shah, N.G., Wach, A., Brachat, A., Philippsen, P.,
1156 and Pringle, J.R. (1998). Additional modules for versatile and economical PCR-based gene
1157 deletion and modification in Saccharomyces cerevisiae. Yeast *14*, 953-961.

1158 Lucas, M.F., Rousseau, D.L., and Guallar, V. (2011). Electron transfer pathways in cytochrome c
1159 oxidase. Biochim Biophys Acta *1807*, 1305-1313.

1160 Luger, K., Mader, A.W., Richmond, R.K., Sargent, D.F., and Richmond, T.J. (1997). Crystal
1161 structure of the nucleosome core particle at 2.8 A resolution. Nature *389*, 251-260.

1162 Luger, K., Rechsteiner, T.J., and Richmond, T.J. (1999). Preparation of nucleosome core particle
1163 from recombinant histones. Method Enzymol *304*, 3-19.

1164 Macadangdang, B.R., Oberai, A., Spektor, T., Campos, O.A., Sheng, F., Carey, M.F., Vogelauer,
1165 M., and Kurdistani, S.K. (2014). Evolution of histone 2A for chromatin compaction in eukaryotes.
1166 Elife *3*, e02792.

1167 Mann, R.K., and Grunstein, M. (1992). Histone H3 N-Terminal Mutations Allow Hyperactivation
1168 of the Yeast Gal1 Gene Invivo. Embo J *11*, 3297-3306.

1169 Mattiroli, F., Bhattacharyya, S., Dyer, P.N., White, A.E., Sandman, K., Burkhart, B.W., Byrne,
1170 K.R., Lee, T., Ahn, N.G., Santangelo, T.J.*, et al.* (2017). Structure of histone-based chromatin in
1171 Archaea. Science *357*, 609-611.

1172 McRae, R., Lai, B., and Fahrni, C.J. (2013). Subcellular redistribution and mitotic inheritance of
1173 transition metals in proliferating mouse fibroblast cells. Metallomics *5*, 52-61.

1174 Mesu, J.G., Visser, T., Soulimani, F., van Faassen, E.E., de Peinder, P., Beale, A.M., and
1175 Weckhuysen, B.M. (2006). New insights into the coordination chemistry and molecular structure
1176 of copper(II) histidine complexes in aqueous solutions. Inorg Chem *45*, 1960-1971.

1177 Nevitt, T., Ohrvik, H., and Thiele, D.J. (2012). Charting the travels of copper in eukaryotes from
1178 yeast to mammals. Biochimica et biophysica acta *1823*, 1580-1593.

1179 Pecci, L., Montefoschi, G., Musci, G., and Cavallini, D. (1997). Novel findings on the copper
1180 catalysed oxidation of cysteine. Amino Acids *13*, 355-367.

1181 Pereira, S.L., Grayling, R.A., Lurz, R., and Reeve, J.N. (1997). Archaeal nucleosomes.
1182 Proceedings of the National Academy of Sciences of the United States of America *94*, 12633-
1183 12637.

1184 Pufahl, R.A., Singer, C.P., Peariso, K.L., Lin, S.J., Schmidt, P.J., Fahrni, C.J., Culotta, V.C.,
1185 PennerHahn, J.E., and OHalloran, T.V. (1997). Metal ion chaperone function of the soluble Cu(I)
1186 receptor Atx1. Science *278*, 853-856.

1187 Rae, T.D., Schmidt, P.J., Pufahl, R.A., Culotta, V.C., and O'Halloran, T.V. (1999). Undetectable
1188 intracellular free copper: The requirement of a copper chaperone for superoxide dismutase.
1189 Science *284*, 805-808.

1190 Ramachandran, S., Vogel, L., Strahl, B.D., and Dokholyan, N.V. (2011). Thermodynamic stability
1191 of histone H3 is a necessary but not sufficient driving force for its evolutionary conservation. PLoS
1192 computational biology *7*, e1001042.

1193 Rando, O.J. (2010). Genome-wide mapping of nucleosomes in yeast. Methods in enzymology *470*,
1194 105-118.

1195 Ryan, O.W., Skerker, J.M., Maurer, M.J., Li, X., Tsai, J.C., Poddar, S., Lee, M.E., DeLoache, W.,
1196 Dueber, J.E., Arkin, A.P.*, et al.* (2014). Selection of chromosomal DNA libraries using a multiplex
1197 CRISPR system. Elife *3*, e03703.

1198 Saavedra, R.A. (1986). Histones and Metal-Binding Domains. Science *234*, 1589-1589.

1199 Saito, M.A., Sigman, D.M., and Morel, F.M.M. (2003). The bioinorganic chemistry of the ancient
1200 ocean: the co-evolution of cyanobacterial metal requirements and biogeochemical cycles at the
1201 Archean-Proterozoic boundary? Inorg Chim Acta *356*, 308-318.

1202 Sandman, K., and Reeve, J.N. (1998). Origin of the eukaryotic nucleus. Science *280*, 501, 503.

1203 Schmitt, M.E., Brown, T.A., and Trumpower, B.L. (1990). A Rapid and Simple Method for
1204 Preparation of Rna from Saccharomyces cerevisiae. Nucleic Acids Res *18*, 3091-3092.

1205 Solomon, E.I., Lowery, M.D., LaCroix, L.B., and Root, D.E. (1993). Electronic absorption
1206 spectroscopy of copper proteins. Methods in enzymology *226*, 1-33.

1207 Spinazzi, M., Casarin, A., Pertegato, V., Salviati, L., and Angelini, C. (2012). Assessment of
1208 mitochondrial respiratory chain enzymatic activities on tissues and cultured cells. Nat Protoc *7*,
1209 1235-1246.

1210 Storici, F., and Resnick, M.A. (2006). The delitto perfetto approach to in vivo site-directed
1211 mutagenesis and chromosome rearrangements with synthetic oligonucleotides in yeast. Methods
1212 in enzymology *409*, 329-345.

1213 Williams, K.R., Gamelin, D.R., LaCroix, L.B., Houser, R.P., Tolman, W.B., Mulder, T.C., deVries,
1214 S., Hedman, B., Hodgson, K.O., and Solomon, E.I. (1997). Influence of copper-sulfur covalency
1215 and copper-copper bonding on valence delocalization and electron transfer in the Cu-A site of
1216 cytochrome c oxidase. J Am Chem Soc *119*, 613-614.

1217 Winston, G.P., and Jaiser, S.R. (2008). Copper deficiency myelopathy and subacute combined
1218 degeneration of the cord - Why is the phenotype so similar? Med Hypotheses *71*, 229-236.

1219 Xu, G., Deng, N., Zhao, Z., Judeh, T., Flemington, E., and Zhu, D. (2011). SAMMate: a GUI tool
1220 for processing short read alignments in SAM/BAM format. Source code for biology and medicine
1221 *6*, 2.

1222 Yang, L.C., McRae, R., Henary, M.M., Patel, R., Lai, B., Vogt, S., and Fahrni, C.J. (2005). Imaging
1223 of the intracellular topography of copper with a fluorescent sensor and by synchrotron x-ray
1224 fluorescence microscopy. Proceedings of the National Academy of Sciences of the United States
1225 of America *102*, 11179-11184.
1226

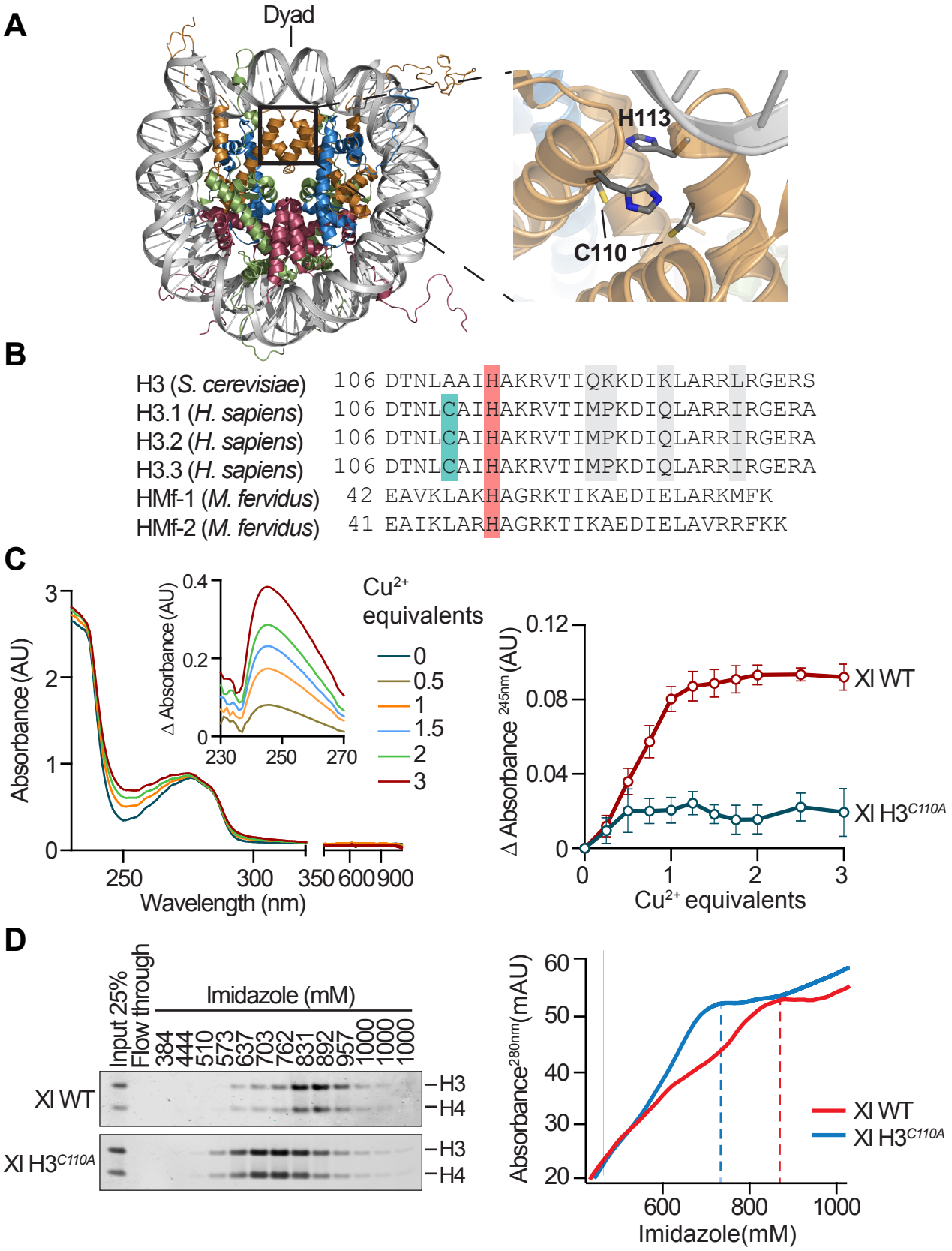
A
Dyad
H113
C110
B
H3 (S. cerevisiae) 106 DTNLAAIHAKRVTIQKKDIKLARRLRGERS
H3.1 (H. sapiens) 106 DTNLCAIHAKRVTIMPKDIQLARRIRGERA
H3.2 (H. sapiens) 106 DTNLCAIHAKRVTIMPKDIQLARRIRGERA
H3.3 (H. sapiens) 106 DTNLCAIHAKRVTIMPKDIQLARRIRGERA
HMf-1 (M. fervidus) 42 EAVKLAKHAGRKTIKAEDIELARKMFK
HMf-2 (M. fervidus) 41 EAIKLARHAGRKTIKAEDIELAVRRFKK
C
Absorbance (AU)
Wavelength (nm)
Δ Absorbance (AU)
Cu2+ equivalents
0
0.5
1
1.5
2
3
Δ Absorbance 245nm (AU)
Xl WT
Xl H3C110A
Cu2+ equivalents
D
Input 25%
Flow through
Imidazole (mM)
384
444
510
573
637
703
762
831
892
957
1000
1000
1000
Xl WT
Xl H3C110A
H3
H4
Absorbance280nm(mAU)
Imidazole(mM)

Figure 1

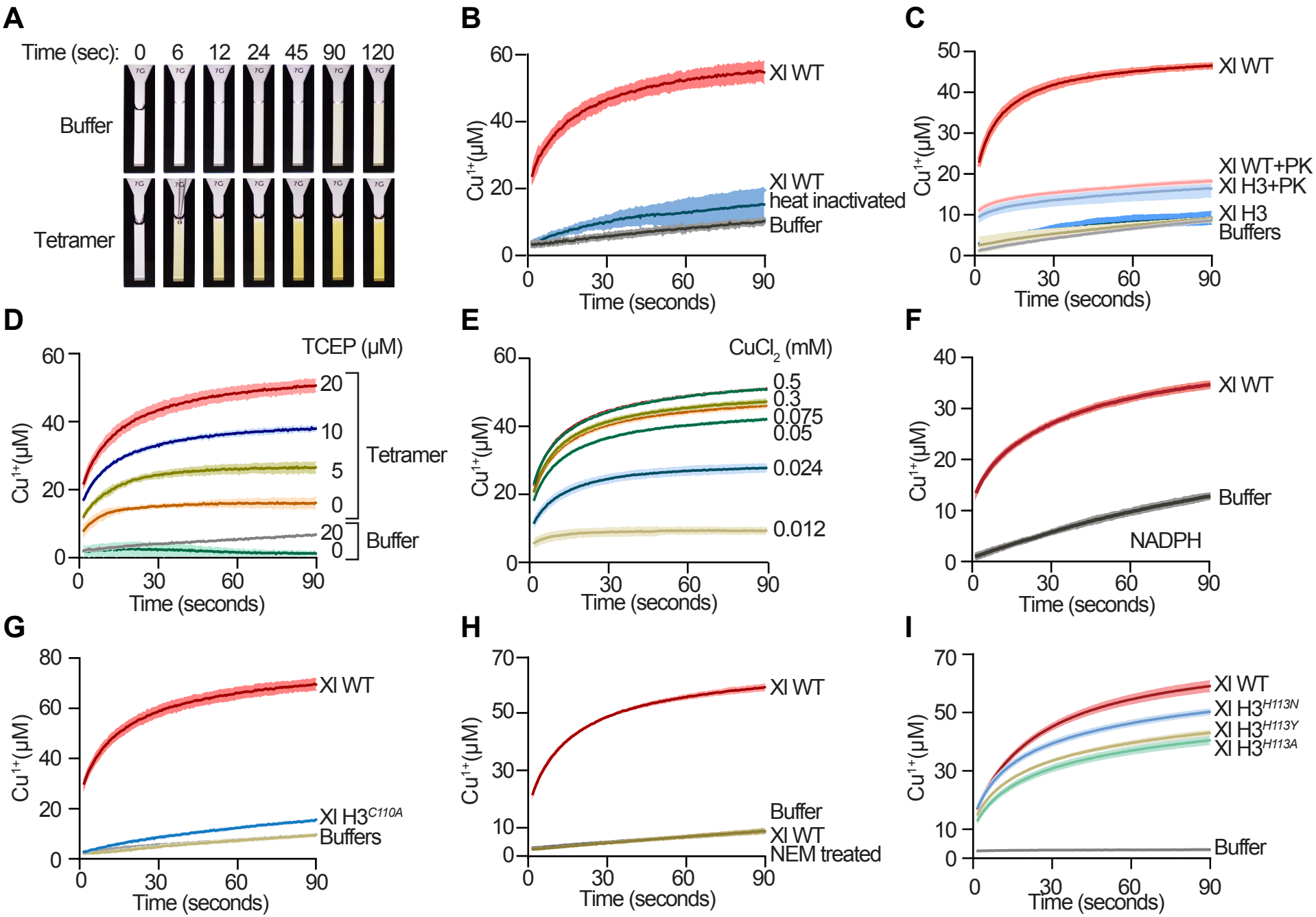
A
Time (sec): 0 6 12 24 45 90 120
Buffer
Tetramer
B
Cu1+(μM)
Time (seconds)
XI WT
XI WT
heat inactivated
Buffer
C
Cu1+(μM)
Time (seconds)
XI WT
XI WT+PK
XI H3+PK
XI H3
Buffers
D
TCEP (μM)
Cu1+(μM)
Time (seconds)
20
10
5
0
Tetramer
20
0
Buffer
E
CuCl2 (mM)
Cu1+(μM)
Time (seconds)
0.5
0.3
0.075
0.05
0.024
0.012
F
Cu1+(μM)
Time (seconds)
XI WT
Buffer
NADPH
G
Cu1+(μM)
Time (seconds)
XI WT
XI H3C110A
Buffers
H
Cu1+(μM)
Time (seconds)
XI WT
Buffer
XI WT
NEM treated
I
Cu1+(μM)
Time (seconds)
XI WT
XI H3H113N
XI H3H113Y
XI H3H113A
Buffer

Figure 2

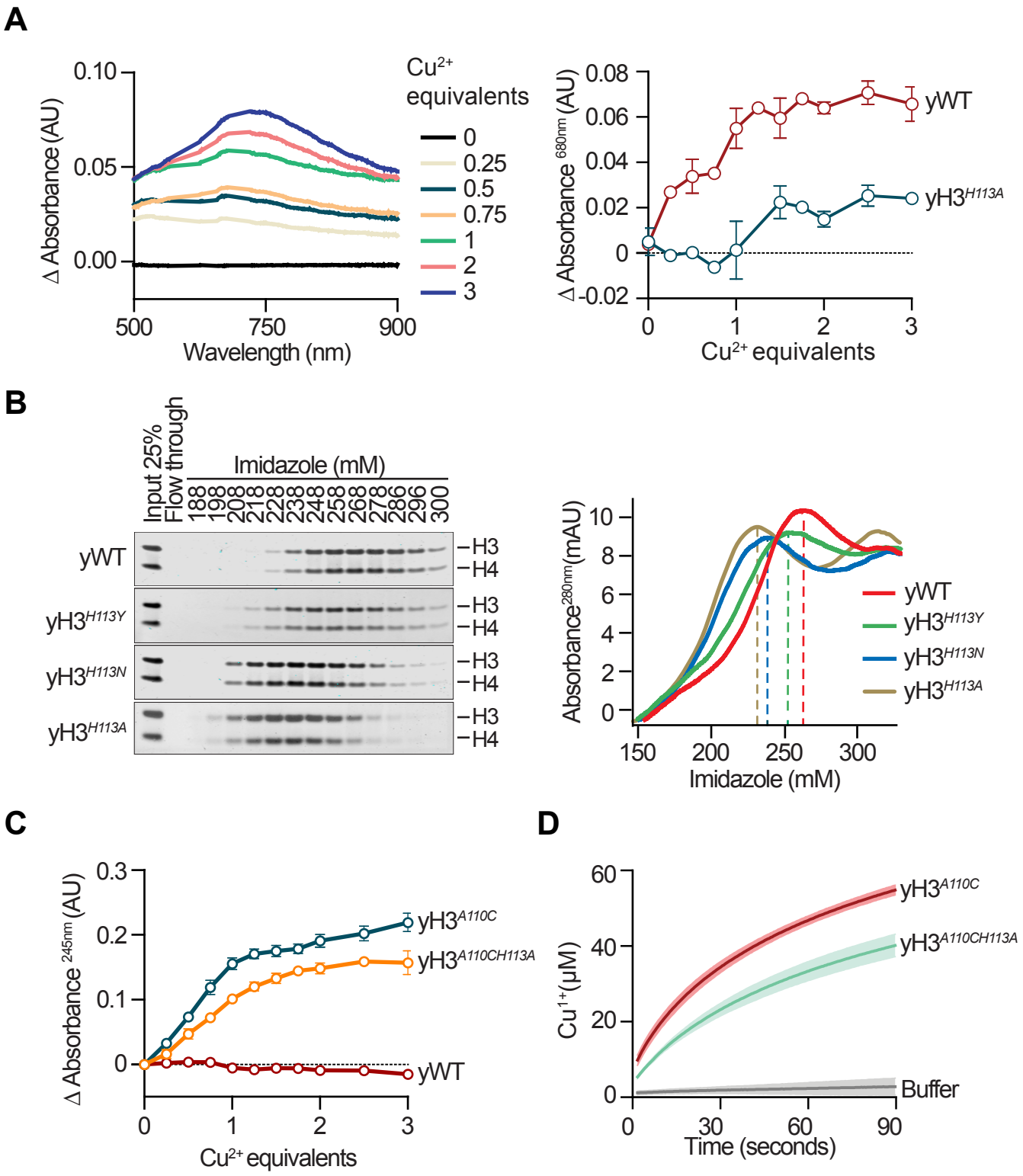
A
0.10
0.05
0.00
Δ Absorbance (AU)
500
750
900
Wavelength (nm)
Cu2+ equivalents
0
0.25
0.5
0.75
1
2
3
0.08
0.06
0.04
0.02
0
-0.02
Δ Absorbance 680nm (AU)
0
1
2
3
Cu2+ equivalents
yWT
yH3H113A
B
Input 25%
Flow through
Imidazole (mM)
188
198
208
218
228
238
248
258
268
278
286
296
300
yWT
yH3H113Y
yH3H113N
yH3H113A
H3
H4
10
8
6
4
2
0
Absorbance280nm(mAU)
150
200
250
300
Imidazole (mM)
yWT
yH3H113Y
yH3H113N
yH3H113A
C
0.3
0.2
0.1
0
Δ Absorbance 245nm (AU)
0
1
2
3
Cu2+ equivalents
yH3A110C
yH3A110CH113A
yWT
D
60
40
20
0
Cu1+(μM)
0
30
60
90
Time (seconds)
yH3A110C
yH3A110CH113A
Buffer

Figure 3

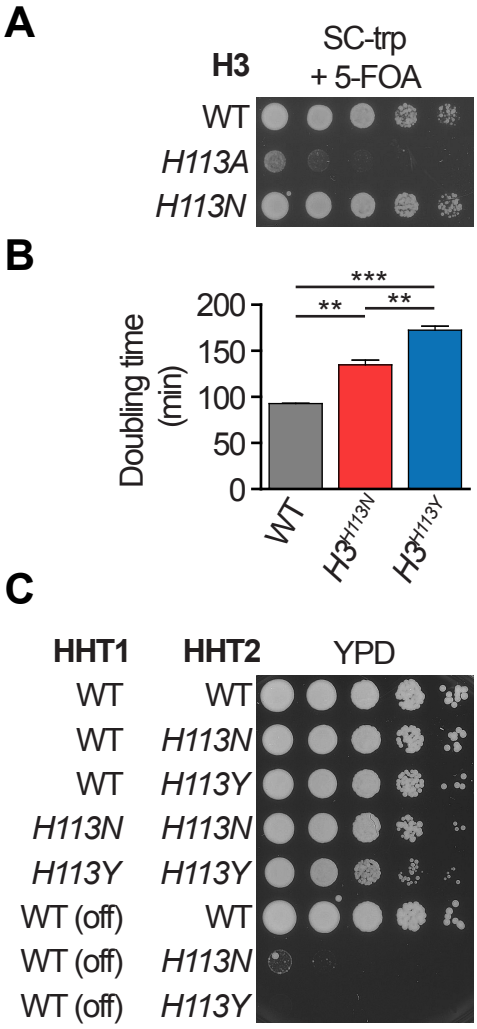
A
H3
SC-trp
+ 5-FOA
WT
H113A
H113N
B
Doubling time
(min)
200
150
100
50
0
***
**
**
WT
H3H113N
H3H113Y
C
HHT1
HHT2
YPD
WT
WT
WT
H113N
H113Y
WT (off)
WT (off)
WT (off)
WT
H113N
H113Y
H113N
H113Y
WT
H113N
H113Y

Figure 4

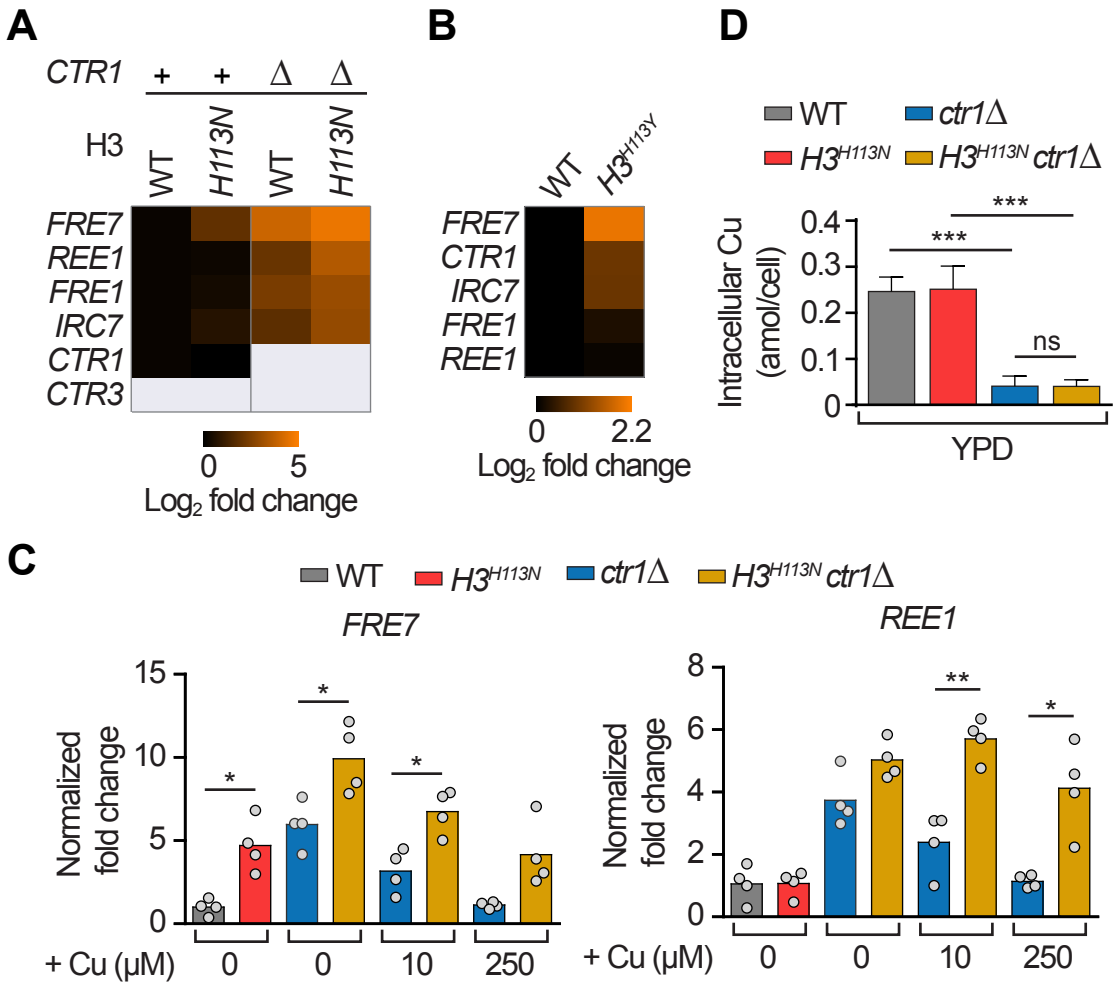
A
CTR1
+
+
Δ
Δ
H3
WT
H113N
WT
H113N
FRE7
REE1
FRE1
IRC7
CTR1
CTR3
0
5
Log2 fold change
B
WT
H3H113Y
FRE7
CTR1
IRC7
FRE1
REE1
0
2.2
Log2 fold change
D
WT
ctr1Δ
H3H113N
H3H113N ctr1Δ
Intracellular Cu (amol/cell)
0.4
0.3
0.2
0.1
0
***
***
ns
YPD
C
WT
H3H113N
ctr1Δ
H3H113N ctr1Δ
FRE7
REE1
Normalized fold change
15
10
5
0
*
*
*
+ Cu (μM)
0
0
10
250
8
6
4
2
0
**
*
+ Cu (μM)
0
0
10
250

Figure 5

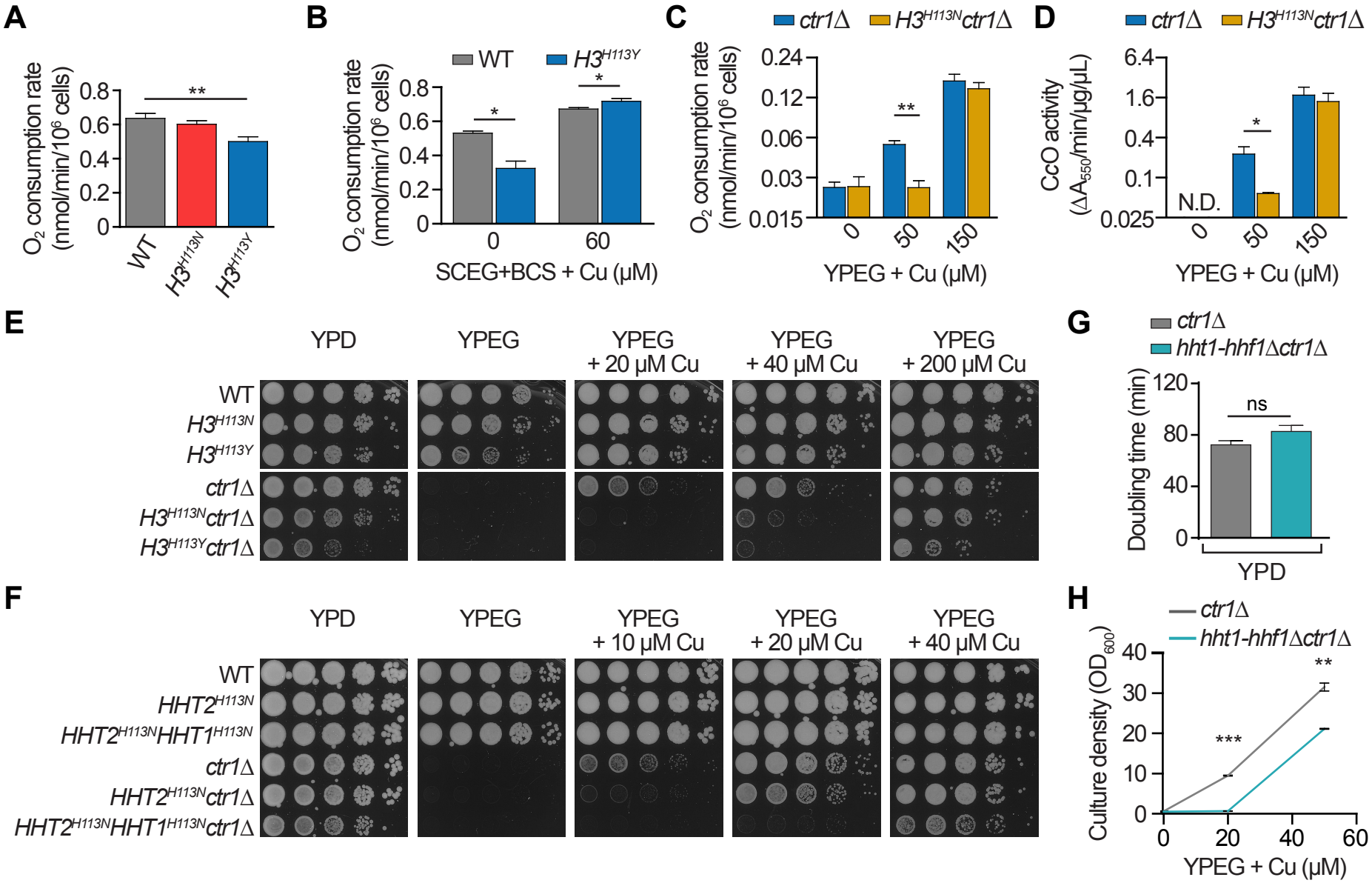
A
O2 consumption rate (nmol/min/10^6 cells)
0.8
0.6
0.4
0.2
0
**
WT
H3H113N
H3H113Y
B
WT
H3H113Y
O2 consumption rate (nmol/min/10^6 cells)
0.8
0.6
0.4
0.2
0
*
*
0
60
SCEG+BCS + Cu (μM)
C
ctr1Δ
H3H113Nctr1Δ
O2 consumption rate (nmol/min/10^6 cells)
0.24
0.12
0.06
0.03
0.015
**
0
50
150
YPEG + Cu (μM)
D
ctr1Δ
H3H113Nctr1Δ
CcO activity (ΔA550/min/μg/μL)
6.4
1.6
0.4
0.1
0.025
N.D.
*
0
50
150
YPEG + Cu (μM)
E
YPD
YPEG
YPEG + 20 μM Cu
YPEG + 40 μM Cu
YPEG + 200 μM Cu
WT
H3H113N
H3H113Y
ctr1Δ
H3H113Nctr1Δ
H3H113Yctr1Δ
G
ctr1Δ
hht1-hhf1Δctr1Δ
Doubling time (min)
120
80
40
0
ns
YPD
F
YPD
YPEG
YPEG + 10 μM Cu
YPEG + 20 μM Cu
YPEG + 40 μM Cu
WT
HHT2H113N
HHT2H113NHHT1H113N
ctr1Δ
HHT2H113Nctr1Δ
HHT2H113NHHT1H113Nctr1Δ
H
ctr1Δ
hht1-hhf1Δctr1Δ
Culture density (OD600)
40
30
20
10
0
***
**
0
20
40
60
YPEG + Cu (μM)

Figure 6

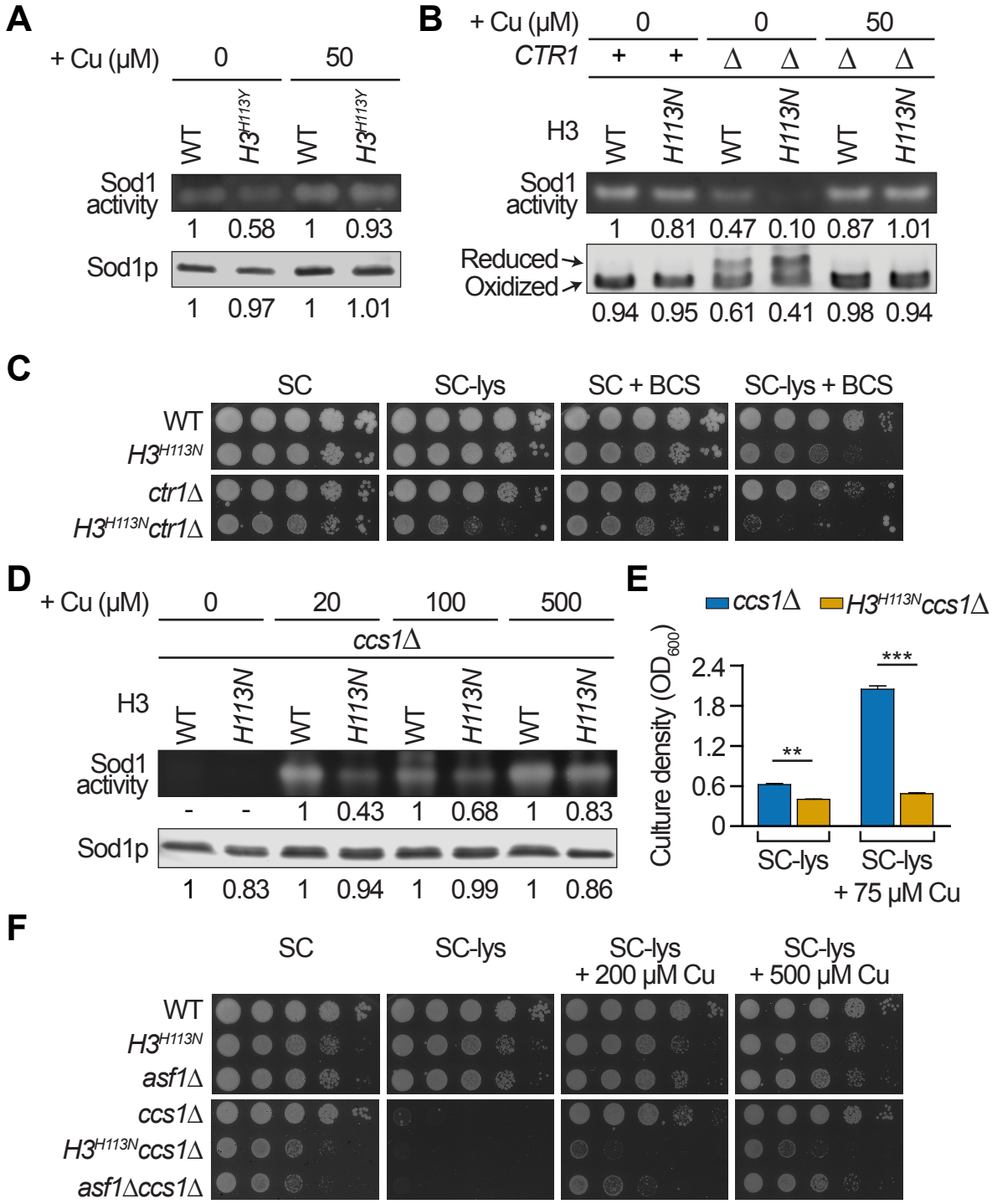
A
+ Cu (μM)
0
50
WT
H3H113Y
WT
H3H113Y
Sod1 activity
1 0.58 1 0.93
Sod1p
1 0.97 1 1.01
B
+ Cu (μM)
0
0
50
CTR1
+ + Δ Δ Δ Δ
H3
WT H113N WT H113N WT H113N
Sod1 activity
1 0.81 0.47 0.10 0.87 1.01
Reduced
Oxidized
0.94 0.95 0.61 0.41 0.98 0.94
C
SC
SC-lys
SC + BCS
SC-lys + BCS
WT
H3H113N
ctr1Δ
H3H113Nctr1Δ
D
+ Cu (μM)
0
20
100
500
ccs1Δ
H3
WT H113N WT H113N WT H113N WT H113N
Sod1 activity
- - 1 0.43 1 0.68 1 0.83
Sod1p
1 0.83 1 0.94 1 0.99 1 0.86
E
ccs1Δ
H3H113Nccs1Δ
Culture density (OD600)
2.4
1.8
1.2
0.6
0
**
***
SC-lys
SC-lys + 75 μM Cu
F
SC
SC-lys
SC-lys + 200 μM Cu
SC-lys + 500 μM Cu
WT
H3H113N
asf1Δ
ccs1Δ
H3H113Nccs1Δ
asf1Δccs1Δ

Figure 7

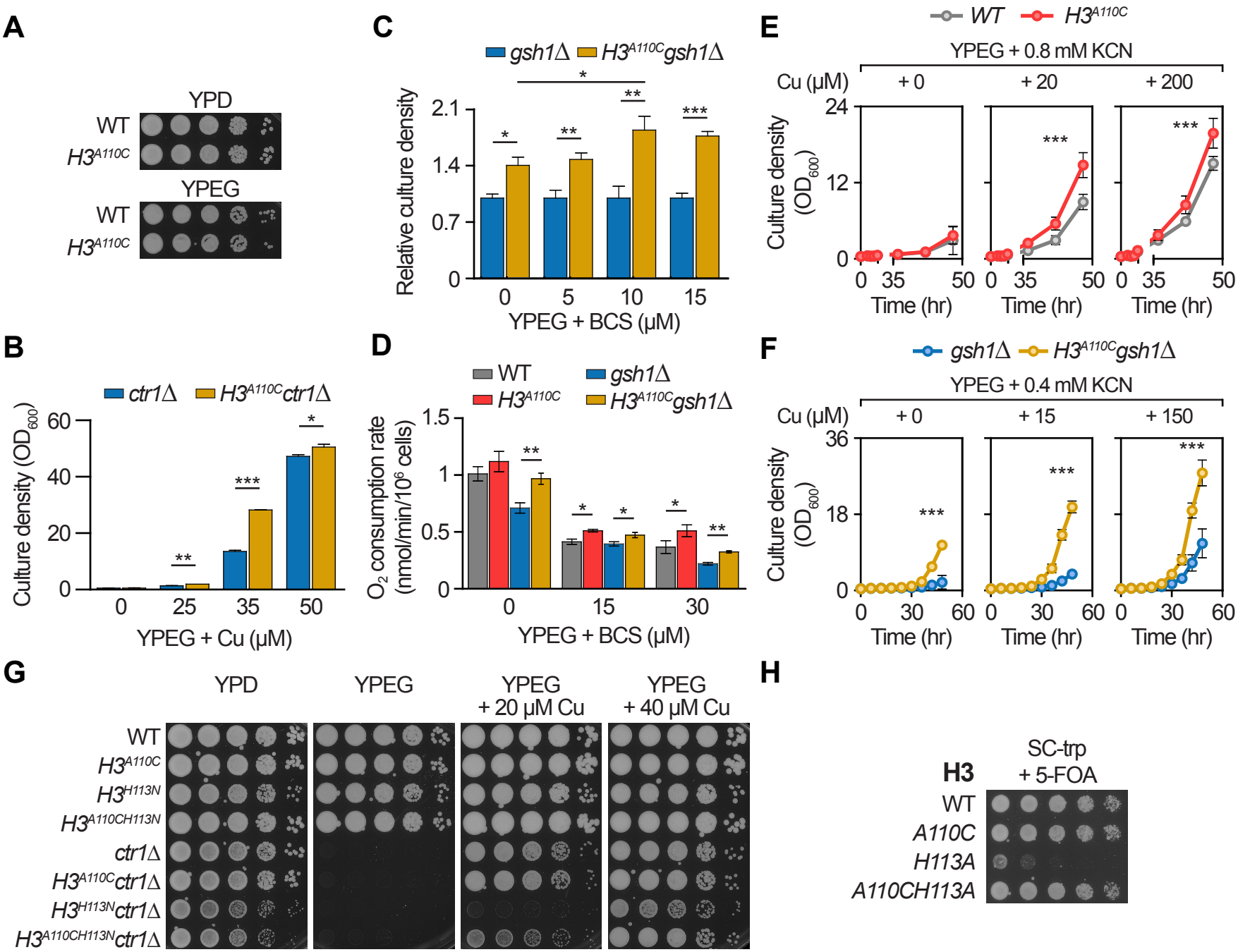
A
YPD
WT
H3A110C
YPEG
WT
H3A110C
B
ctr1Δ
H3A110Cctr1Δ
Culture density (OD600)
60
40
20
0
0
25
35
50
YPEG + Cu (μM)
C
gsh1Δ
H3A110Cgsh1Δ
Relative culture density
2.1
1.4
0.7
0
0
5
10
15
YPEG + BCS (μM)
D
WT
gsh1Δ
H3A110C
H3A110Cgsh1Δ
O2 consumption rate (nmol/min/10^6 cells)
1.5
1
0.5
0
0
15
30
YPEG + BCS (μM)
E
WT
H3A110C
YPEG + 0.8 mM KCN
Cu (μM)
+ 0
+ 20
+ 200
Culture density (OD600)
24
12
0
0
35
50
Time (hr)
F
gsh1Δ
H3A110Cgsh1Δ
YPEG + 0.4 mM KCN
Cu (μM)
+ 0
+ 15
+ 150
Culture density (OD600)
36
18
0
0
30
60
Time (hr)
G
YPD
YPEG
YPEG + 20 μM Cu
YPEG + 40 μM Cu
WT
H3A110C
H3H113N
H3A110CH113N
ctr1Δ
H3A110Cctr1Δ
H3H113Nctr1Δ
H3A110CH113Nctr1Δ
H
H3
SC-trp + 5-FOA
WT
A110C
H113A
A110CH113A

Figure 8

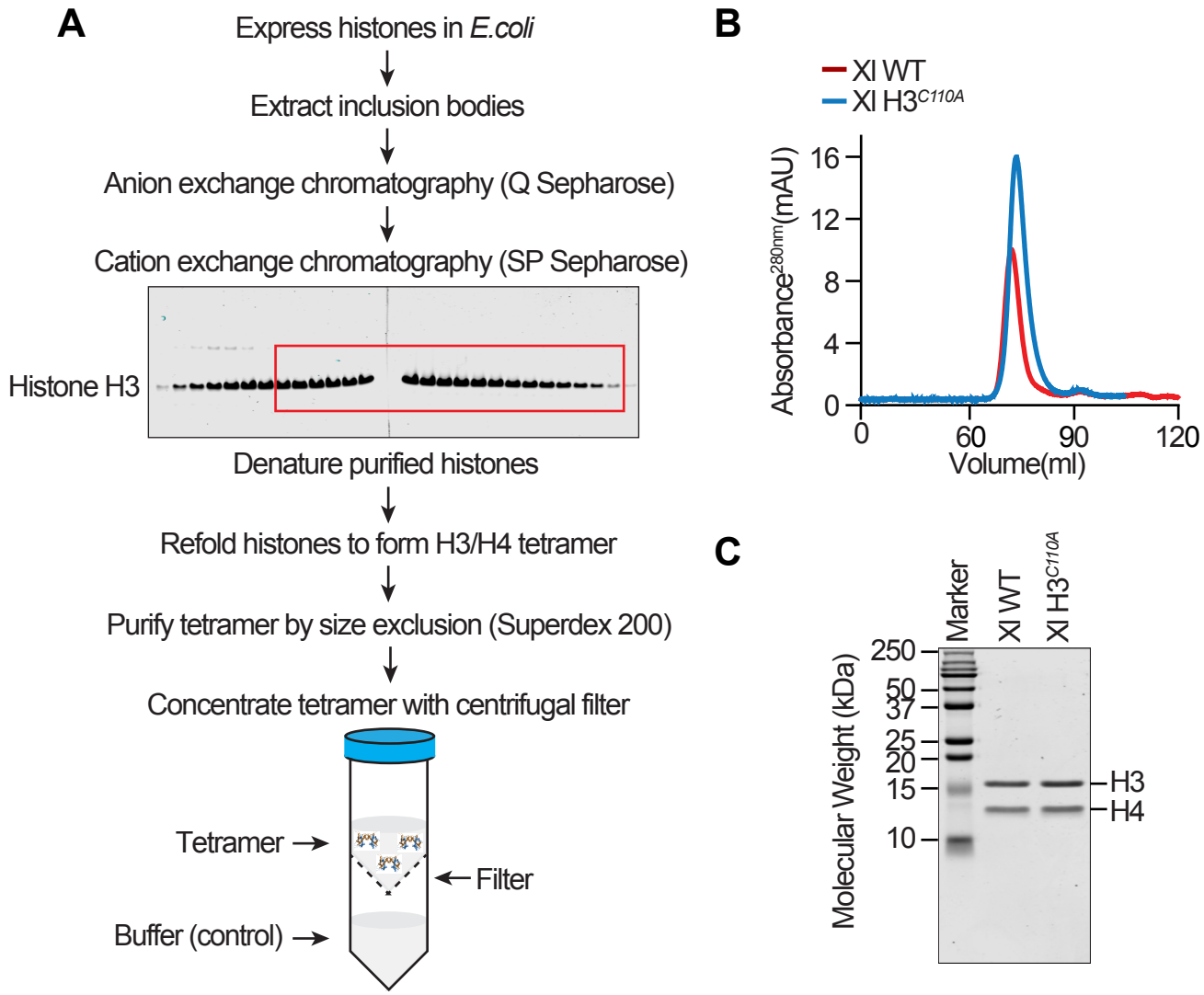

Figure 1 - figure supplement 1

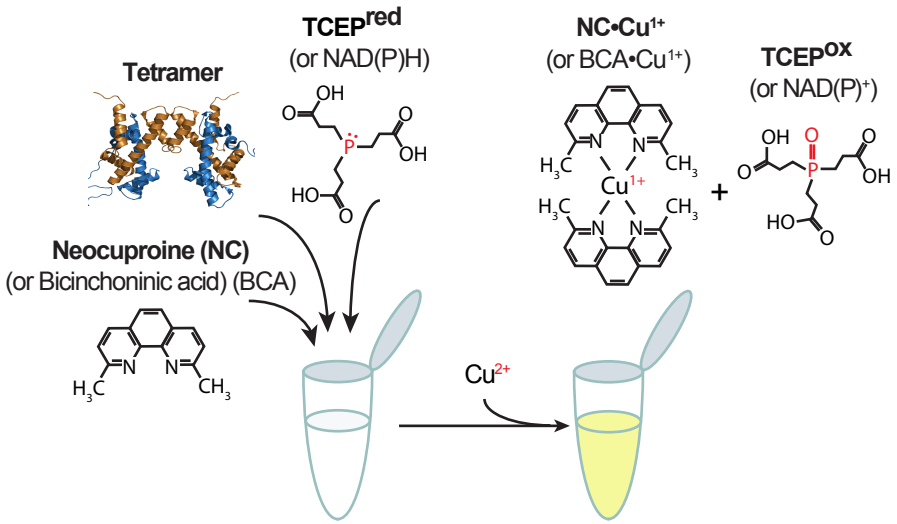

Figure 2 - figure supplement 1

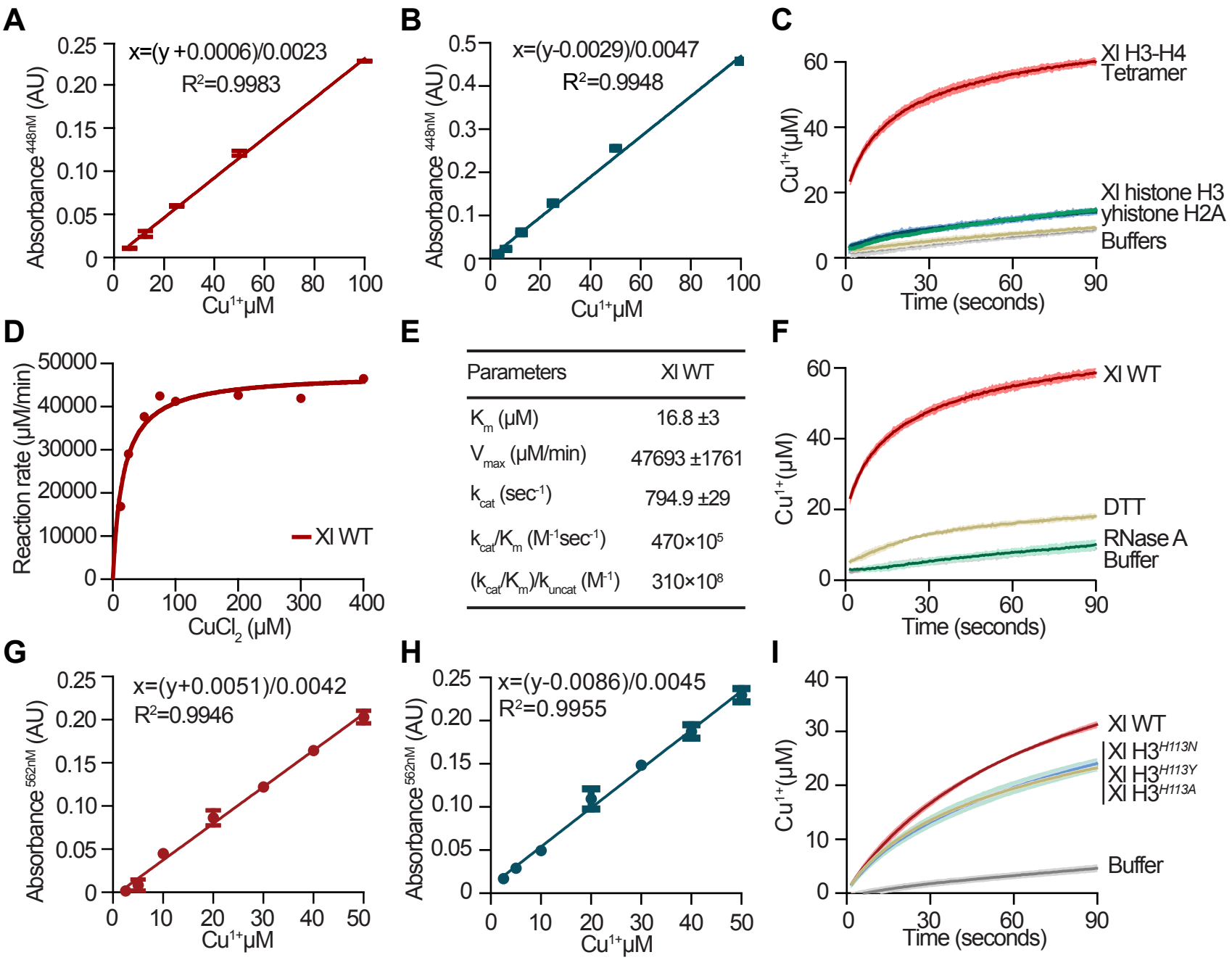

Parameters	XI WT
K_m (µM)	16.8 ±3
V_{max} (µM/min)	47693 ±1761
k_{cat} (sec^{-1})	794.9 ±29
k_{cat}/K_m ($M^{-1}sec^{-1}$)	470×10^5
$(k_{cat}/K_m)/k_{uncat}$ (M^{-1})	310×10^8

Figure 2 - figure supplement 2

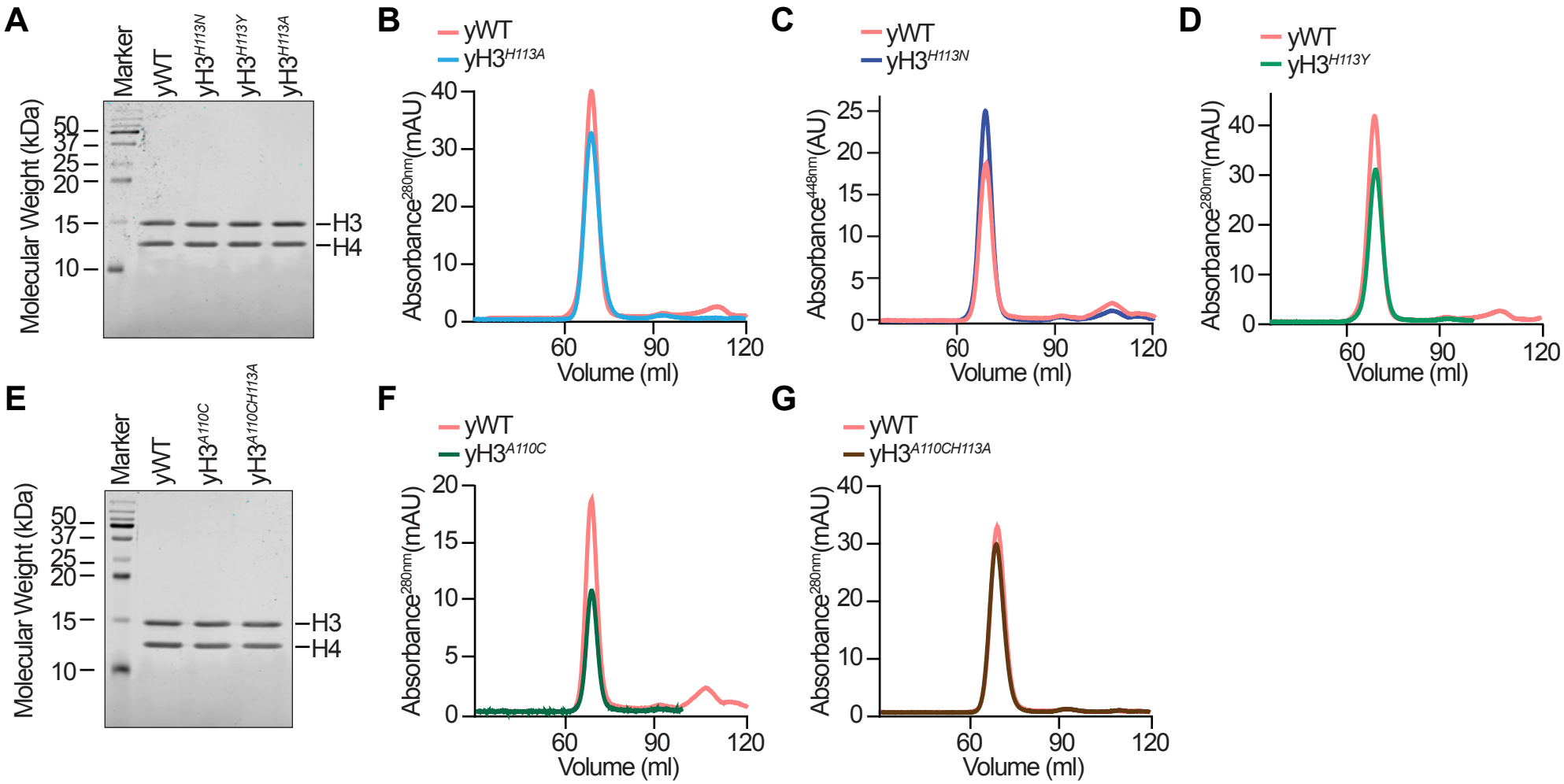

Figure 3 - figure supplement 1

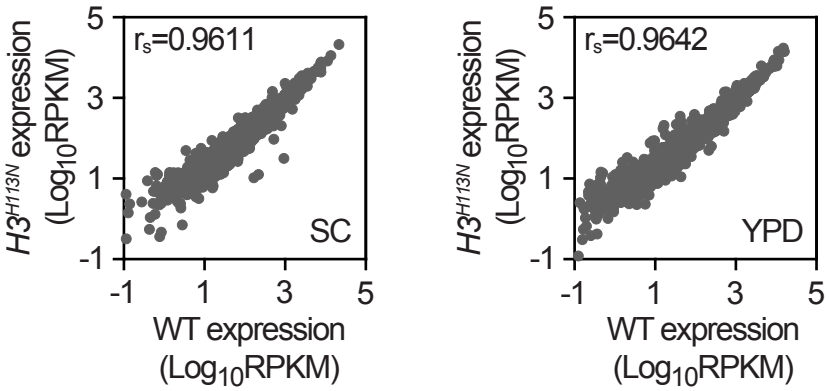

Figure 5 - figure supplement 1

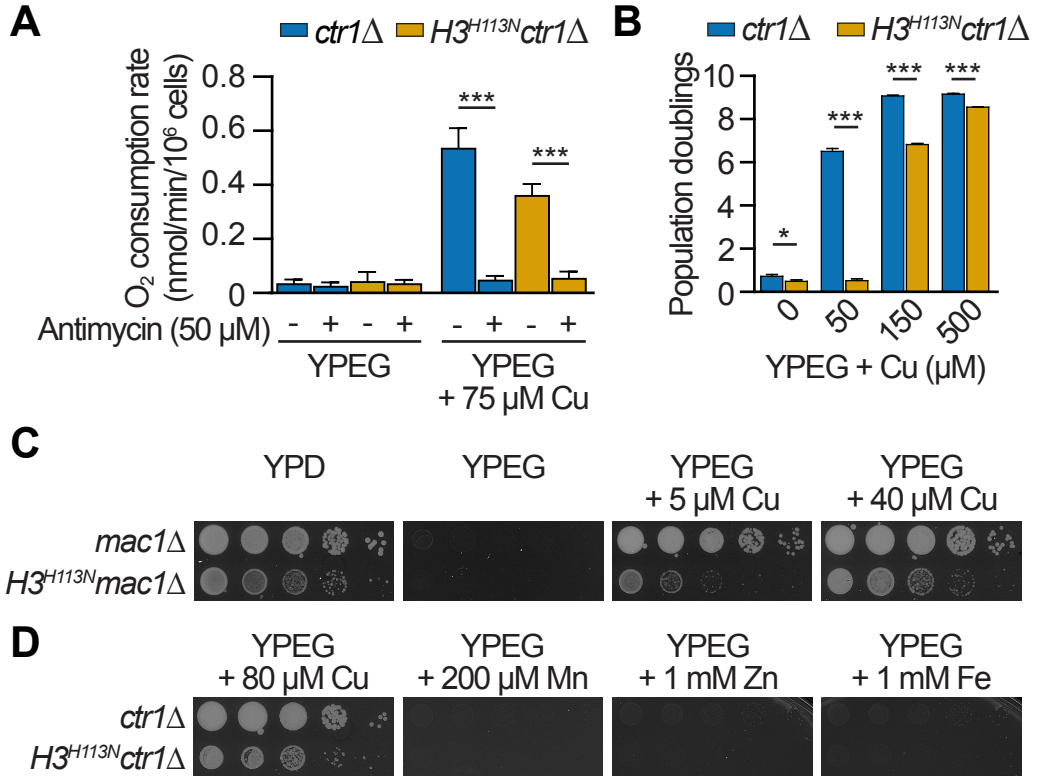

Figure 6 - figure supplement 1

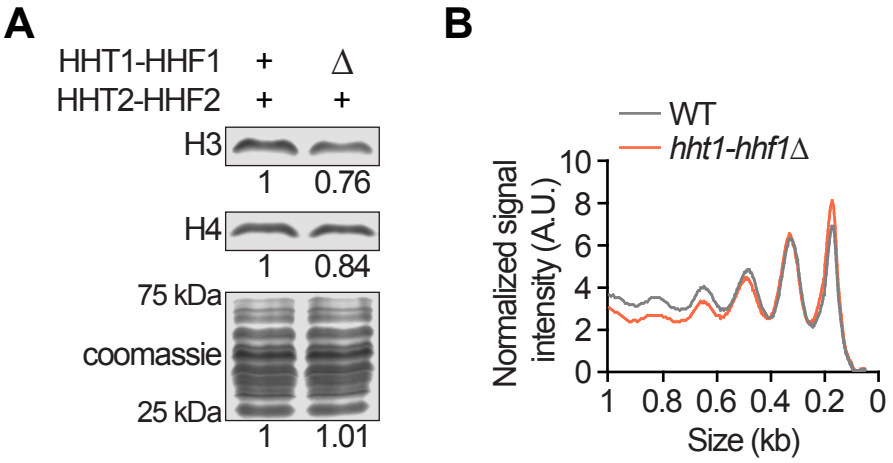

Figure 6 - figure supplement 2

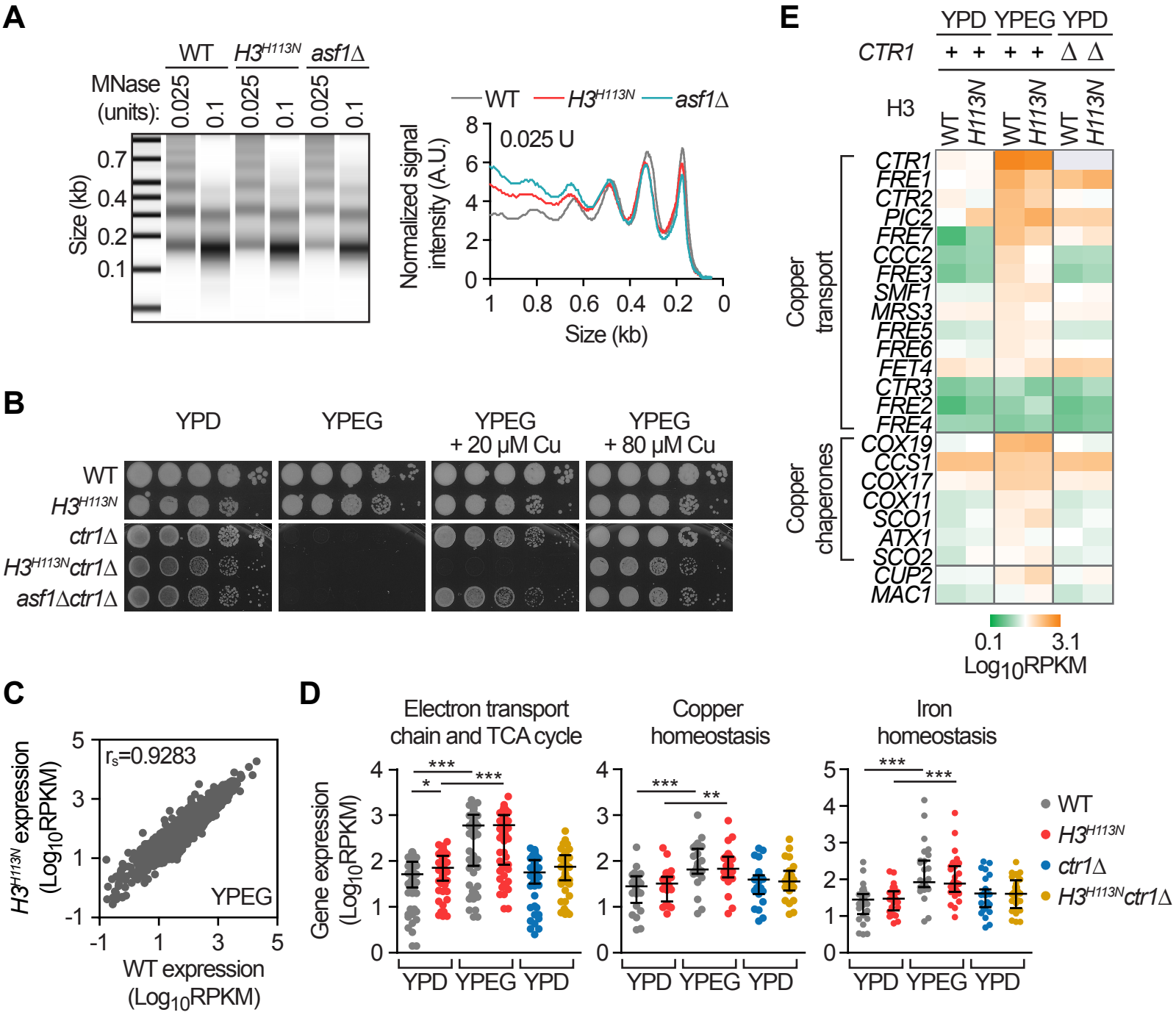

Figure 6 - figure supplement 3

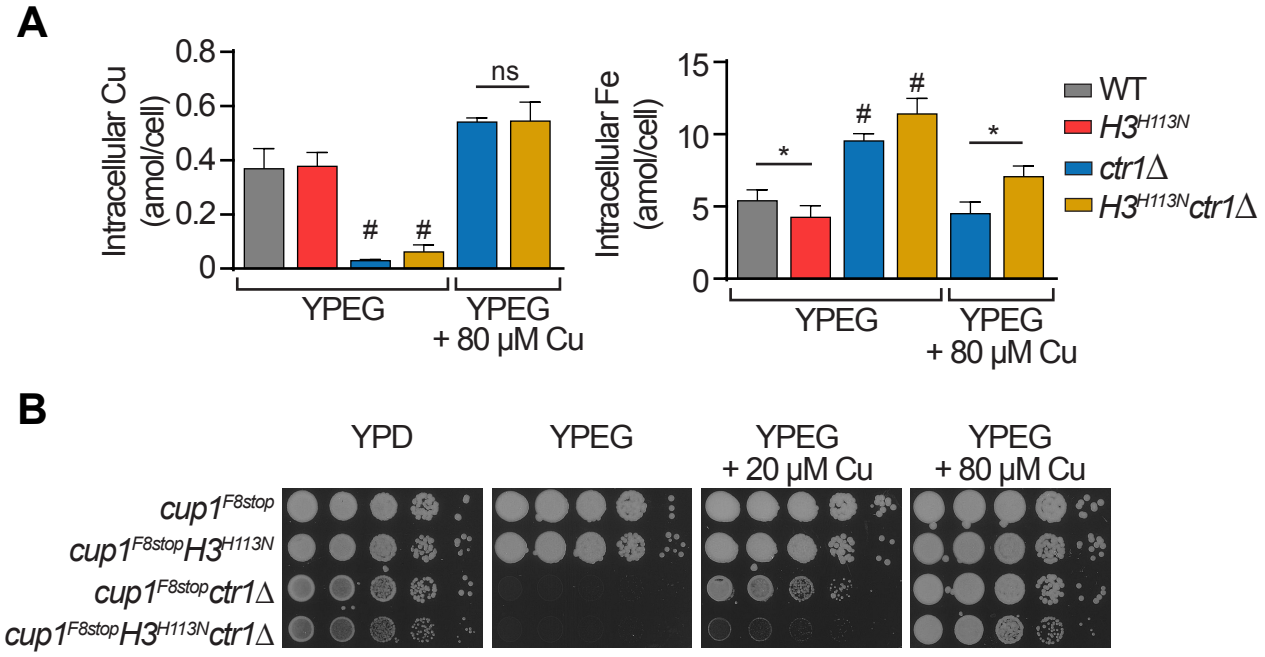

Figure 6 - figure supplement 4

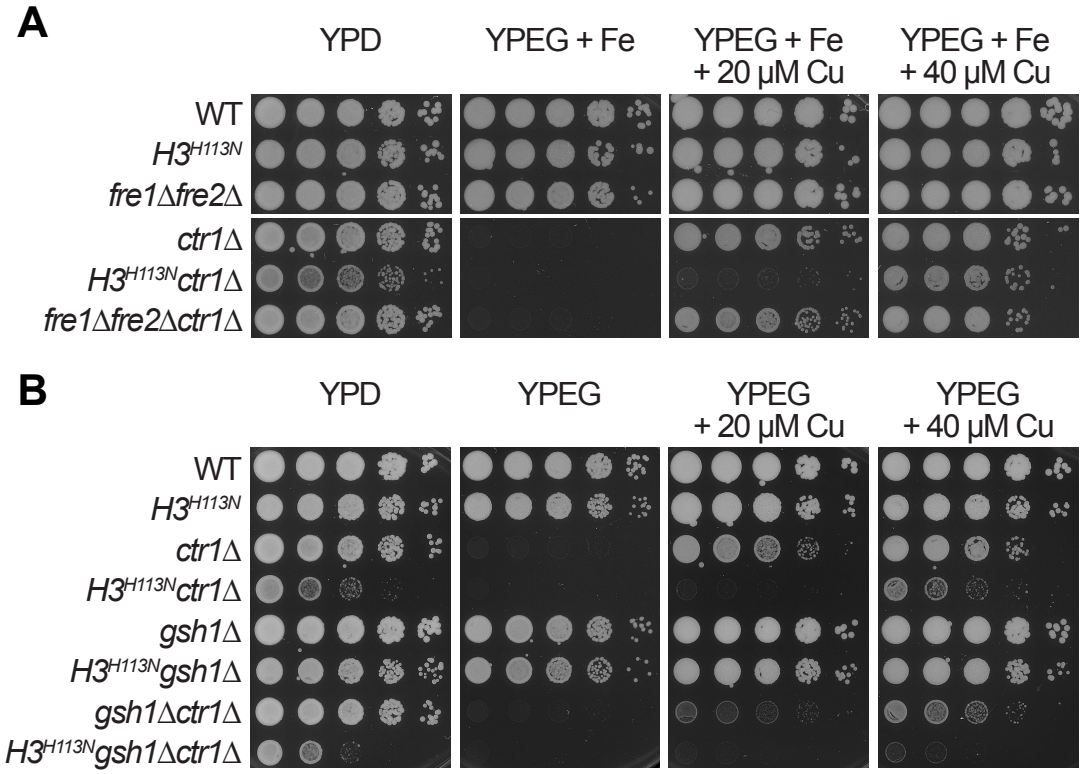

Figure 6 - figure supplement 5

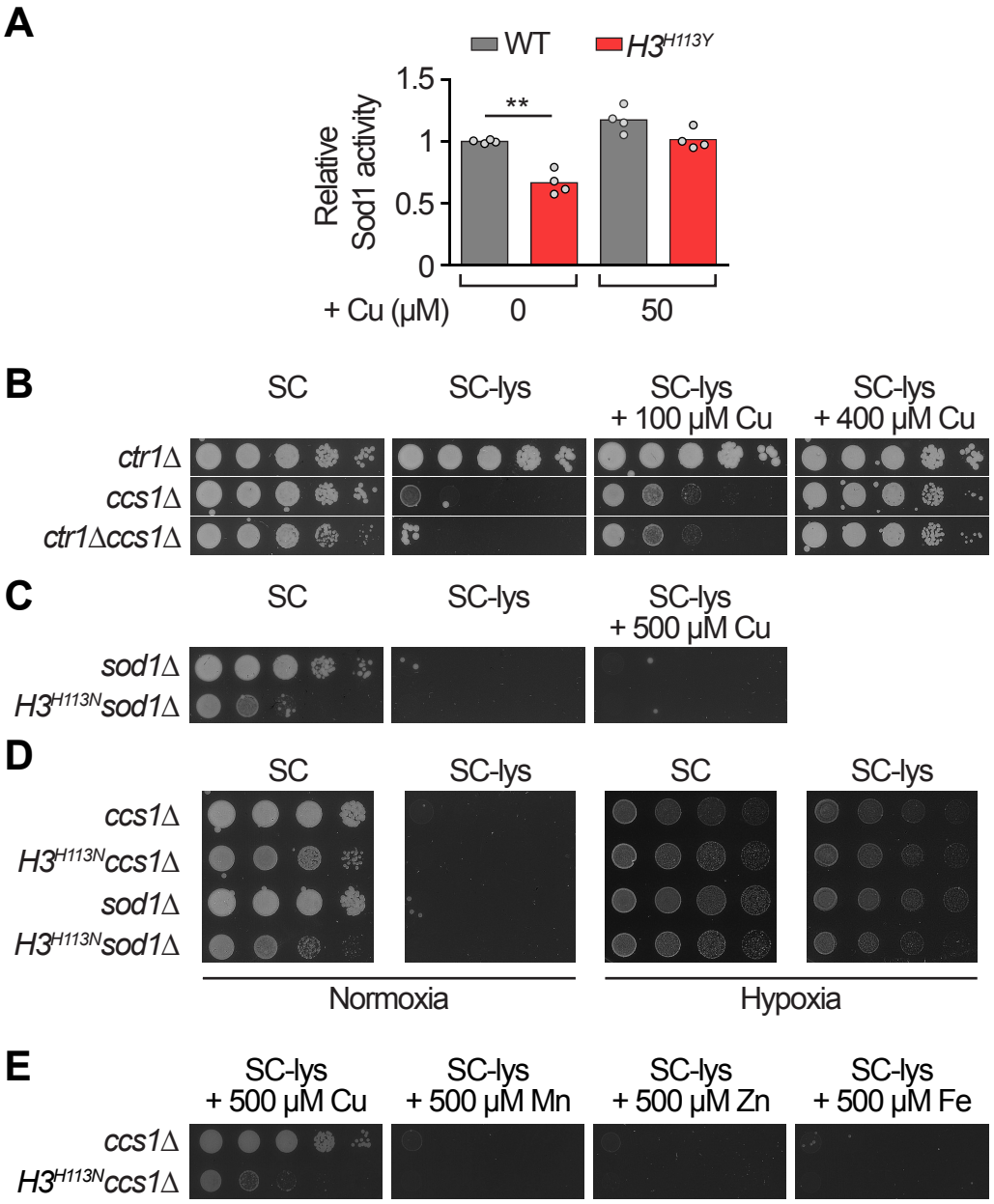

Figure 7 - figure supplement 1

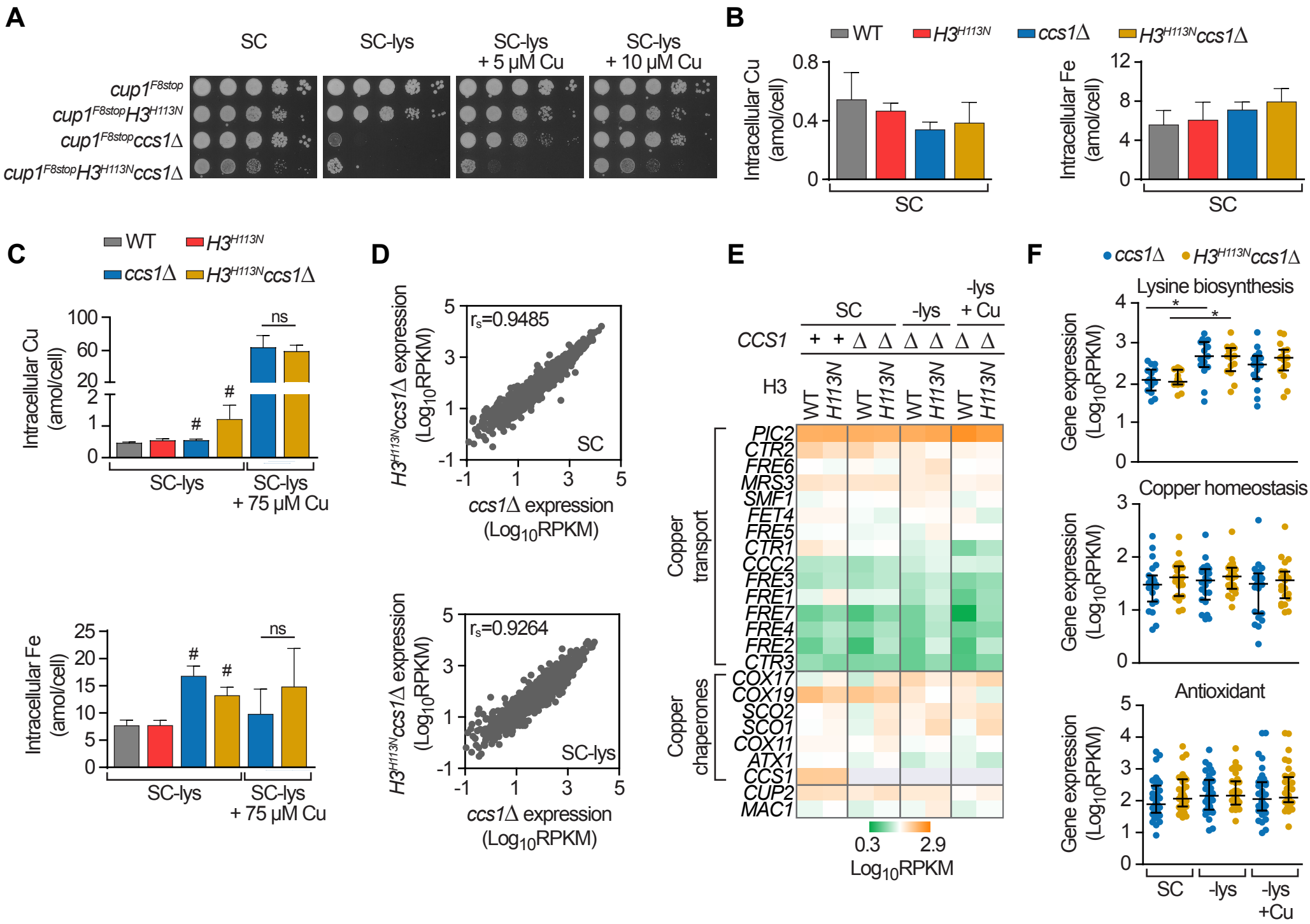

Figure 7 - figure supplement 2

Table 1 | Yeast strains used in this study

Strain name	Mutant short name	Genotype	Reference
BY4741	parental	*MATa his3Δ1 leu2Δ0 met15Δ0 ura3Δ0*	Brachmann et al., 1998
OCY1131	WT	*MATa his3Δ1 leu2Δ0 met15Δ0 ura3Δ0, (hht2Δ::ura3)Δ::HHT2*	This study
OCY1136	$H3^{H113N}$	*MATa his3Δ1 leu2Δ0 met15Δ0 ura3Δ0, (hht2Δ::ura3)Δ::hht2-H113N hht1-H113N*	This study
OCY1133	$p^{(GAL1)}$-*HHT1*	*MATa his3Δ1 leu2Δ0 met15Δ0 ura3Δ0, (hht2Δ::ura3)Δ::HHT2, KanMX6-PGAL1-HHT1*	This study
OCY1134	$hht2^{H113N}p^{(GAL1)}$-*HHT1*	*MATa his3Δ1 leu2Δ0 met15Δ0 ura3Δ0, (hht2Δ::ura3)Δ::hht2-H113N, KanMX6-PGAL1-HHT1*	This study
NAY609	$H3^{H113Y}$	*MATa his3Δ1 leu2Δ0 met15Δ0 ura3Δ0, (hht2Δ::ura3)Δ::HHT2, hht2-H113Y, hht1-H113Y*	This study
NAY616	$H3^{A110C}$	*MATa his3Δ1 leu2Δ0 met15Δ0 ura3Δ0, (hht2Δ::ura3)Δ::HHT2, hht2-A110C, hht1-A110C*	This study
OCY2951	$hht2^{H113Y}p^{(GAL1)}$-*HHT1*	*MATa his3Δ1 leu2Δ0 met15Δ0 ura3Δ0, (hht2Δ::ura3)Δ::HHT2, hht2-H113Y, KanMX6-PGAL1-HHT1*	This study
NAY536	*asf1Δ*	*MATa his3Δ1 leu2Δ0 met15Δ0 ura3Δ0, (hht2::ura3)::HHT2, asf1Δ::HphMX4*	This study
OCY1861	*ctr1Δ*	*MATa his3Δ1 leu2Δ0 met15Δ0 ura3Δ0, (hht2Δ::ura3)Δ::HHT2, ctr1Δ::HphMX4*	This study
OCY1862	$H3^{H113N}$ *ctr1Δ*	*MATa his3Δ1 leu2Δ0 met15Δ0 ura3Δ0, (hht2Δ::ura3)Δ::hht2-H113N hht1-H113N, ctr1Δ::HphMX4*	This study
OCY2141	*asf1Δ ctr1Δ*	*MATa his3Δ1 leu2Δ0 met15Δ0 ura3Δ0, (hht2Δ::ura3)Δ::HHT2, asf1Δ::HphMX4, ctr1Δ::His3MX6*	This study
OCY2251	*mac1Δ*	*MATa his3Δ1 leu2Δ0 met15Δ0 ura3Δ0, (hht2Δ::ura3)Δ::HHT2, mac1Δ::His3MX6*	This study
OCY2252	$H3^{H113N}$ *mac1Δ*	*MATa his3Δ1 leu2Δ0 met15Δ0 ura3Δ0, (hht2Δ::ura3)Δ::hht2-H113N hht1-H113N, mac1Δ::His3MX6*	This study
OCY2621	*ctr1Δ*	*MATa his3Δ1 leu2Δ0 met15Δ0 ura3Δ0, (hht2Δ::ura3)Δ::HHT2, ctr1Δ*	This study
OCY2622	$H3^{H113N}$ *ctr1Δ*	*MATa his3Δ1 leu2Δ0 met15Δ0 ura3Δ0, (hht2Δ::ura3)Δ::hht2-H113N hht1-H113N, ctr1Δ*	This study
OCY2623	$H3^{H113Y}$ *ctr1Δ*	*MATa his3Δ1 leu2Δ0 met15Δ0 ura3Δ0, (hht2Δ::ura3)Δ::HHT2, hht2-H113Y, hht1-H113Y, ctr1Δ*	This study
OCY1981	$cup1^{F8stop}$	*MATa his3Δ1 leu2Δ0 met15Δ0 ura3Δ0, (hht2Δ::ura3)Δ::HHT2, cup1-F8stop*	This study
OCY1983	$cup1^{F8stop}H3^{H113N}$	*MATa his3Δ1 leu2Δ0 met15Δ0 ura3Δ0, (hht2Δ::ura3)Δ::HHT2, cup1-F8stop, hht1-H113N hht2-H113N*	This study
OCY2181	$cup1^{F8stop}$*ctr1Δ*	*MATa his3Δ1 leu2Δ0 met15Δ0 ura3Δ0, (hht2Δ::ura3)Δ::HHT2, cup1-F8stop, ctr1Δ::His3MX6*	This study
OCY2182	$cup1^{F8stop}H3^{H113N}$*ctr1Δ*	*MATa his3Δ1 leu2Δ0 met15Δ0 ura3Δ0, (hht2Δ::ura3)Δ::HHT2, cup1-F8stop, hht1-H113N hht2-H113N, ctr1Δ::His3MX6*	This study
OCY1132	$hht2^{H113N}$	*MATa his3Δ1 leu2Δ0 met15Δ0 ura3Δ0, (hht2Δ::ura3)Δ::hht2-H113N*	This study
OCY2628	$hht2^{H113N}$*ctr1Δ*	*MATa his3Δ1 leu2Δ0 met15Δ0 ura3Δ0, (hht2Δ::ura3)Δ::hht2-H113N, ctr1Δ*	This study
NAY553	*ccs1Δ*	*MATa his3Δ1 leu2Δ0 met15Δ0 ura3Δ0, (hht2::ura3)::HHT2, ccs1Δ::KanMX6*	This study
NAY554	$H3^{H113N}$ *ccs1Δ*	*MATa his3Δ1 leu2Δ0 met15Δ0 ura3Δ0, (hht2::ura3)::hht2-H113N hht1-H113N, ccs1Δ::KanMX6*	This study
NAY597	*asf1Δ ccs1Δ*	*MATa his3Δ1 leu2Δ0 met15Δ0 ura3Δ0, (hht2Δ::ura3)Δ::HHT2, asf1Δ::HphMX4, ccs1Δ::His3MX6*	This study
NAY551	*sod1Δ*	*MATa his3Δ1 leu2Δ0 met15Δ0 ura3Δ0, (hht2::ura3)::HHT2, sod1Δ::HphMX4*	This study
NAY552	$H3^{H113N}$ *sod1Δ*	*MATa his3Δ1 leu2Δ0 met15Δ0 ura3Δ0, (hht2::ura3)::hht2-H113N hht1-H113N, sod1Δ::HphMX4*	This study
OCY2211	$cup1^{F8stop}$*ccs1Δ*	*MATa his3Δ1 leu2Δ0 met15Δ0 ura3Δ0, (hht2Δ::ura3)Δ::HHT2, cup1-F8stop, ccs1Δ::KanMX6*	This study
OCY2212	$cup1^{F8stop}H3^{H113N}$*ccs1Δ*	*MATa his3Δ1 leu2Δ0 met15Δ0 ura3Δ0, (hht2Δ::ura3)Δ::HHT2, cup1-F8stop, hht1-H113N hht2-H113N, ccs1Δ::KanMX6*	This study
OCY1135	*hht1-hhf1Δ*	*MATa his3Δ1 leu2Δ0 met15Δ0 ura3Δ0, (hht2Δ::ura3)Δ::HHT2, hht1-hhf1Δ::HphMX4*	This study
OCY2421	*ctr1Δ*	*MATa his3Δ1 leu2Δ0 met15Δ0 ura3Δ0, (hht2Δ::ura3)Δ::HHT2, ctr1Δ::His3MX6*	This study
NAY564	*hht1-hhf1Δctr1Δ*	*MATa his3Δ1 leu2Δ0 met15Δ0 ura3Δ0, (hht2Δ::ura3)Δ::HHT2, hht1-hhf1Δ::HphMX4, ctr1Δ::His3MX6*	This study
OCY2781	*fre1Δfre2Δ*	*MATa his3Δ1 leu2Δ0 met15Δ0 ura3Δ0 (hht2Δ::ura3)Δ::HHT2, fre1Δ::KanMX6, fre2Δ::His3MX6*	This study
OCY2791	*fre1Δfre2Δctr1Δ*	*MATa his3Δ1 leu2Δ0 met15Δ0 ura3Δ0 (hht2Δ::ura3)Δ::HHT2, fre1Δ::KanMX6, fre2Δ::His3MX6, ctr1Δ*	This study
OCY2371	*gsh1Δ*	*MATa his3Δ1 leu2Δ0 met15Δ0 ura3Δ0, (hht2Δ::ura3)Δ::HHT2, gsh1Δ::KanMX6*	This study
OCY2372	$H3^{H113N}$*gsh1Δ*	*MATa his3Δ1 leu2Δ0 met15Δ0 ura3Δ0, (hht2Δ::ura3)Δ::hht2-H113N hht1-H113N, gsh1Δ::KanMX6*	This study
OCY2373	$H3^{A110C}$*gsh1Δ*	*MATa his3Δ1 leu2Δ0 met15Δ0 ura3Δ0, (hht2Δ::ura3)Δ::hht2-A110C hht1-A110C, gsh1Δ::KanMX6*	This study
OCY2626	$H3^{A110C}$*ctr1Δ*	*MATa his3Δ1 leu2Δ0 met15Δ0 ura3Δ0, (hht2Δ::ura3)Δ::HHT2, hht2-A110C, hht1-A110C, ctr1Δ*	This study
OCY2671	$H3^{A110CH113N}$	*MATa his3Δ1 leu2Δ0 met15Δ0 ura3Δ0 (hht2Δ::ura3)Δ::HHT2, hht2-A110CH113N, hht1-A110CH113N*	This study
OCY2627	$H3^{A110CH113N}$*ctr1Δ*	*MATa his3Δ1 leu2Δ0 met15Δ0 ura3Δ0 (hht2Δ::ura3)Δ::HHT2, hht2-A110CH113N, hht1-A110CH113N, ctr1Δ*	This study
RMY102	parental	*MATa ade2-101 his3-Δ200 lys2-801 trp1Δ901 ura3-52 (hht1-hhf1)Δ::LEU2 (hht2-hhf2)Δ::HIS3 pRM102[CEN4 ARS1 URA3 pGAL1-HHT2-pGAL10-HHF2]*	Mann & Grunstein, 1998
NAY702	WT	*MATa ade2-101 his3-Δ200 lys2-801 trp1Δ901 ura3-52 (hht1-hhf1)Δ::LEU2 (hht2-hhf2)Δ::HIS3 pRM102[CEN4 ARS1 URA3 pGAL1-HHT2-pGAL10-HHF2] pRM200[CEN4 ARS1 TRP1 HHT2 HHF2]*	This study
NAY700	*H3-H113A*	*MATa ade2-101 his3-Δ200 lys2-801 trp1Δ901 ura3-52 (hht1-hhf1)Δ::LEU2 (hht2-hhf2)Δ::HIS3 pRM102[CEN4 ARS1 URA3 pGAL1-HHT2-pGAL10-HHF2] pSZ008[CEN4 ARS1 TRP1 hht2-H113A HHF2]*	This study
NAY703	*H3-H113N*	*MATa ade2-101 his3-Δ200 lys2-801 trp1Δ901 ura3-52 (hht1-hhf1)Δ::LEU2 (hht2-hhf2)Δ::HIS3 pRM102[CEN4 ARS1 URA3 pGAL1-HHT2-pGAL10-HHF2] pYX55a[CEN4 ARS1 TRP1 hht2-H113N HHF2]*	This study

NAY701	*H3-A110C*	*MATa ade2-101 his3-Δ200 lys2-801 trp1Δ901 ura3-52 (hht1-hhf1)Δ::LEU2 (hht2-hhf2)Δ::HIS3 pRM102[CEN4 ARS1 URA3 pGAL1-HHT2-pGAL10-HHF2] pSZ011[CEN4 ARS1 TRP1 hht2-A110C HHF2]*	This study
NAY704	*H3-A110CH113A*	*MATa ade2-101 his3-Δ200 lys2-801 trp1Δ901 ura3-52 (hht1-hhf1)Δ::LEU2 (hht2-hhf2)Δ::HIS3 pRM102[CEN4 ARS1 URA3 pGAL1-HHT2-pGAL10-HHF2] pNA20a[CEN4 ARS1 TRP1 hht2-A110CH113A HHF2]*	This study